Argonne
NATIONAL LABORATORY

ANL/RERTR/TM-10-41

Comparison and Validation of HEU and LEU Modeling Results to HEU Experimental Benchmark Data for the Massachusetts Institute of Technology MITR Reactor

Nuclear Engineering Division

About Argonne National Laboratory

Argonne is a U.S. Department of Energy laboratory managed by UChicago Argonne, LLC under contract DE-AC02-06CH11357. The Laboratory's main facility is outside Chicago, at 9700 South Cass Avenue, Argonne, Illinois 60439. For information about Argonne and its pioneering science and technology programs, see www.anl.gov.

Availability of This Report

This report is available, at no cost, at http://www.osti.gov/bridge. It is also available on paper to the U.S. Department of Energy and its contractors, for a processing fee, from:

U.S. Department of Energy
Office of Scientific and Technical Information
P.O. Box 62
Oak Ridge, TN 37831-0062
phone (865) 576-8401
fax (865) 576-5728
reports@adonis.osti.gov

ANL/RERTR/TM-10-41

Comparison and Validation of HEU and LEU Modeling Results to HEU Experimental Benchmark Data for the Massachusetts Institute of Technology MITR Reactor

by
E.H. Wilson[1] and T.H. Newton, Jr.[2], coordinating authors
and
A. Bergeron[1], N. Horelik[2], and J.G. Stevens[1]
[1]Nuclear Engineering Division, Argonne National Laboratory
[2]MIT Nuclear Reactor Laboratory and Nuclear Science and Engineering Department

December 10, 2010

Abstract

The Massachusetts Institute of Technology Reactor (MITR-II) is a research reactor in Cambridge, Massachusetts designed primarily for experiments using neutron beam and in-core irradiation facilities. It delivers a neutron flux comparable to current LWR power reactors in a compact 6 MW core using Highly Enriched Uranium (HEU) fuel.

In the framework of its non-proliferation policies, the international community presently aims to minimize the amount of nuclear material available that could be used for nuclear weapons. In this geopolitical context, most research and test reactors both domestic and international have started a program of conversion to the use of Low Enriched Uranium (LEU) fuel. A new type of LEU fuel based on an alloy of uranium and molybdenum (UMo) is expected to allow the conversion of U.S. domestic high performance reactors like the MITR-II reactor.

Towards this goal, comparisons of MCNP5 Monte Carlo neutronic modeling results for HEU and LEU cores have been performed. Validation of the model has been based upon comparison to HEU experimental benchmark data for the MITR-II. The objective of this work was to demonstrate a model which could represent the experimental HEU data, and therefore could provide a basis to demonstrate LEU core performance.

This report presents an overview of MITR-II model geometry and material definitions which have been verified, and updated as required during the course of validation to represent the specifications of the MITR-II reactor. Results of calculations are presented for comparisons to historical HEU start-up data from 1975-1976, and to other experimental benchmark data available for the MITR-II Reactor through 2009.

This report also presents results of steady state neutronic analysis of an all-fresh LEU fueled core. Where possible, HEU and LEU calculations were performed for conditions equivalent to HEU experiments, which serves as a starting point for safety analyses for conversion of MITR-II from the use of HEU fuel to the use of UMo LEU fuel.

Table of Contents

Table of Contents (continued)

List of Figures

List of Tables

1 Introduction

The Massachusetts Institute of Technology Reactor (MITR-II) is a research reactor in Cambridge, Massachusetts designed primarily for experiments using neutron beam and in-core irradiation facilities. It delivers a neutron flux comparable to current LWR power reactors in a compact 6 MW core using Highly Enriched Uranium (HEU) fuel.

In the framework of its non-proliferation policies, the international community presently aims to minimize the amount of nuclear material available that could be used for nuclear weapons. In this geopolitical context, most research and test reactors both domestic and international have started a program of conversion to the use of Low Enriched Uranium (LEU) fuel. A new type of LEU fuel based on an alloy of uranium and molybdenum (UMo) is expected to allow the conversion of compact high performance reactors like the MITR-II reactor.

This report discusses the methods, and model definitions used for comparison and validation of HEU and LEU modeling results to HEU experimental benchmark data for the MITR-II Reactor. In addition, this report presents an overview of the start-up period of the MITR-II reactor and summarizes key results of experimental measurement on the fresh HEU MITR-II core. Calculations with both HEU and LEU model perturbations equivalent to the experiments are presented alongside the measured results.

Additionally, the modern period of MITR-II operation is described by summary of model and fuel composition for this period. Due to the depleted cores with an involved fuel shuffling pattern, the modern reactor period is described with a general description of a 2 year period of operation during 2007 to 2009. As with the start-up period, comparison to measured experimental data is made using the HEU model.

Since the overall objective is completion of analyses towards the conversion of MITR-II from the use of HEU fuel to the use of UMo LEU fuel, the range of model validation encompasses both the type of fresh safety basis calculation found in the MITR HEU SAR [1], and the modern core modeling which will provide a framework for future thermal hydraulic, accident and transient analyses.

2 MITR-II Reactor Model

In this chapter, the MITR-II reactor physical layout and configurations are discussed alongside geometrical representations made in the MNCP5 model. Aspects of the reactor configuration are presented, including a variety of core configurations, both past and present, which have been used to perform computational comparisons to HEU benchmark measurements. Also presented is a proposed LEU core configuration which served as the reference core, in order to evaluate and compare HEU and LEU core characteristics.

2.1 General Description of Reactor Model

The MITR-II facility, shown in Figure 2-1, is currently licensed to operate at 6 MW. The hexagonal core contains twenty-seven fuel locations in three radial rings (inner A, middle B, and outer C), as shown in Figure 2-2. The core is light water moderated and cooled, but is surrounded by a heavy water (D_2O) reflector. Boron impregnated stainless steel control blades are present at the periphery of the core at each side of the hexagon. In addition, fixed absorbers of boron-stainless steel can be installed in the upper portion of the core (approximately twelve inches) in a hexagonal configuration between the A and B fuel rings, as well as in three radial arms extending to the edge of the core. The hexagonal strut and three connected radial arms are collectively referred to as the spider, which has been modeled in the various historical configurations as discussed in section 4.1.1.

Figure 2-1 General view of the MITR-II facility.

2.1.1 Reactor Fuel Loading

Typically at least three of locations are filled with either an in-core experimental facility or a solid aluminum dummy element to reduce power peaking. The remaining locations are filled with standard MITR-II fuel elements. Figure 2-3 shows an image of the MITR core fueled with twenty-two fueled elements, and five solid aluminum dummies.

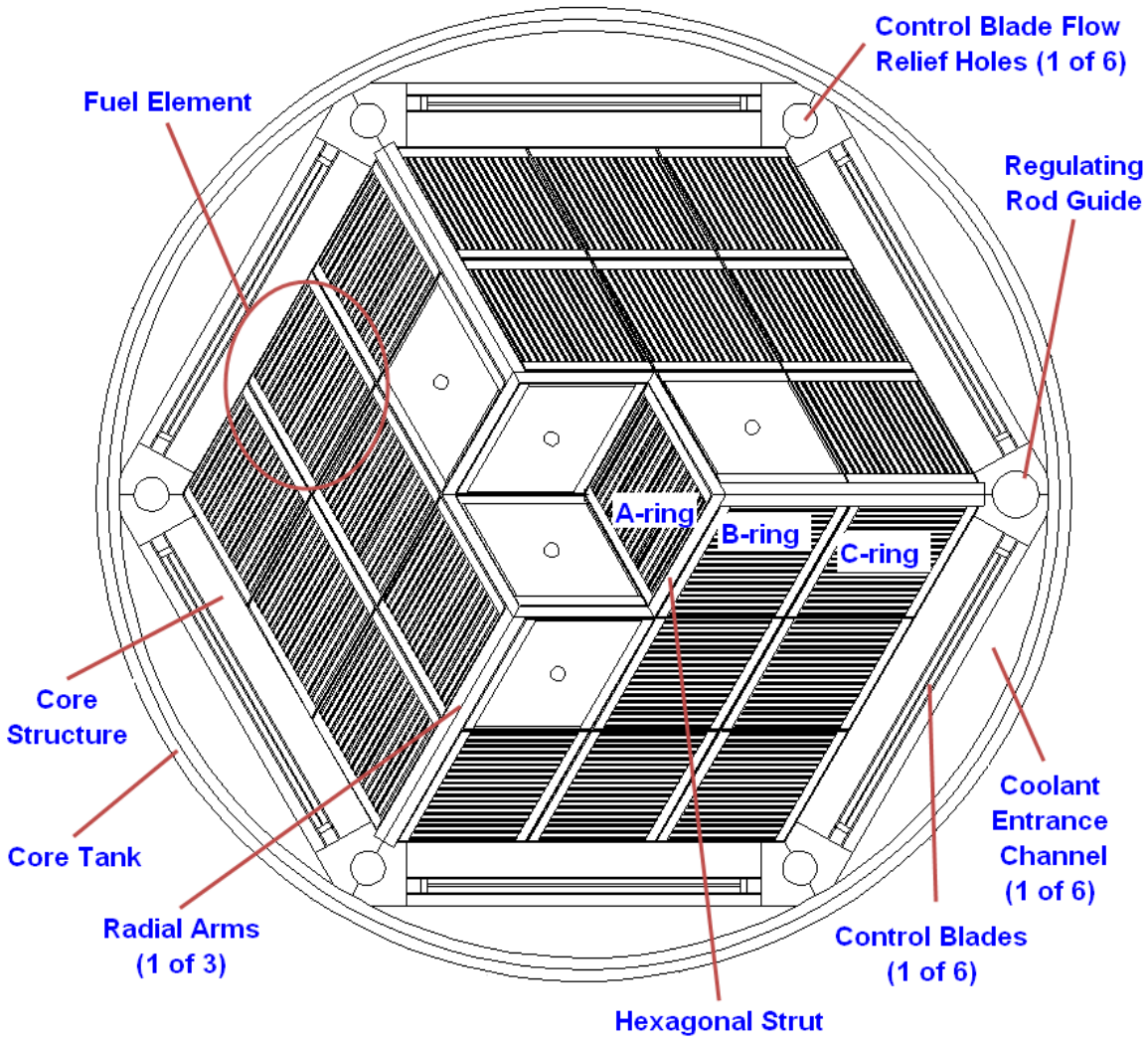

Figure 2-2. Schematic of the reactor core configuration.

2.1.2 Experimental and Ancillary Facilities

Several reentrant thimbles are installed inside the D_2O reflector, delivering greater neutron flux to the beam ports outside the core region. Beyond the D_2O reflector, a secondary reflector of graphite exists in which several horizontal and vertical thermal neutron irradiation facilities are present. In addition, the MITR Fission Converter Facility is installed outside the D_2O reflector. This facility contains eleven partially spent MITR fuel elements for delivery of a beam of primarily epithermal neutrons to the medical facility for use in Boron Neutron Capture Therapy (BNCT). Figure 2-4 shows a larger view of the reactor including the reflector regions and experimental facilities.

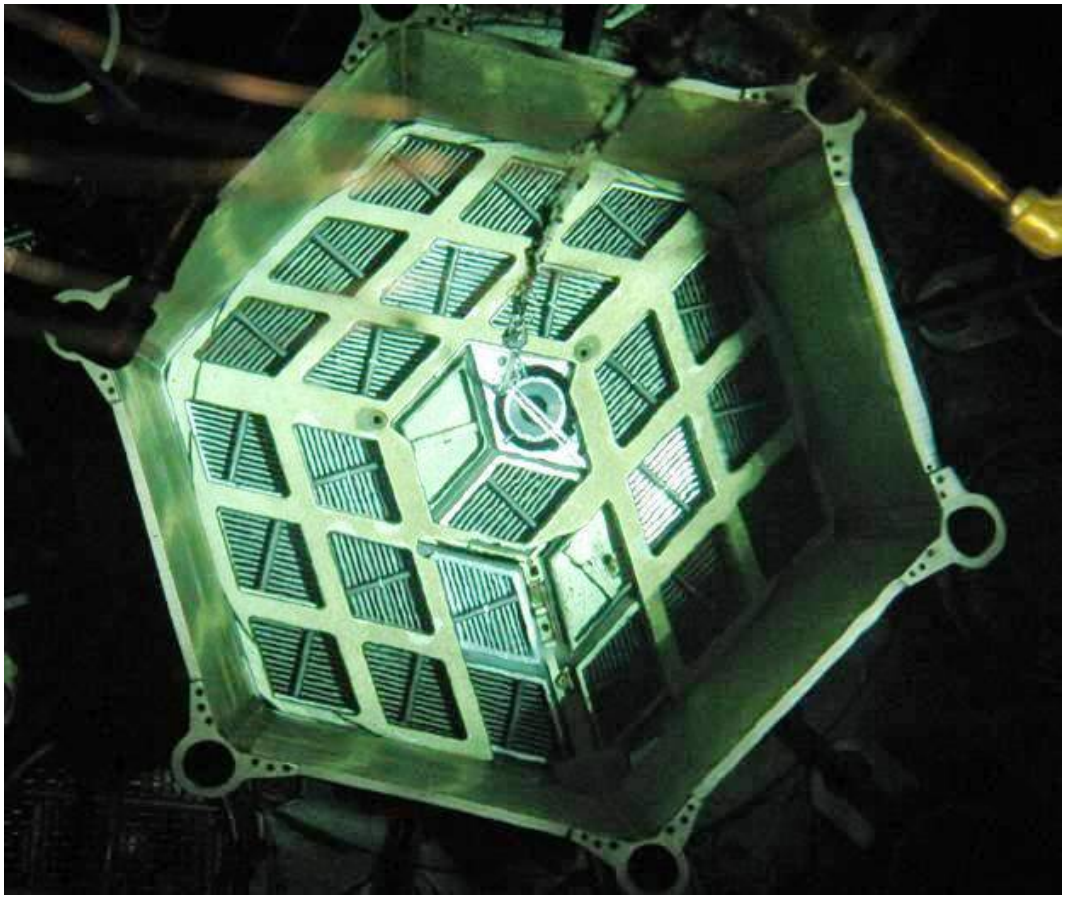

Figure 2-3. Overview of MITR-II core tank.

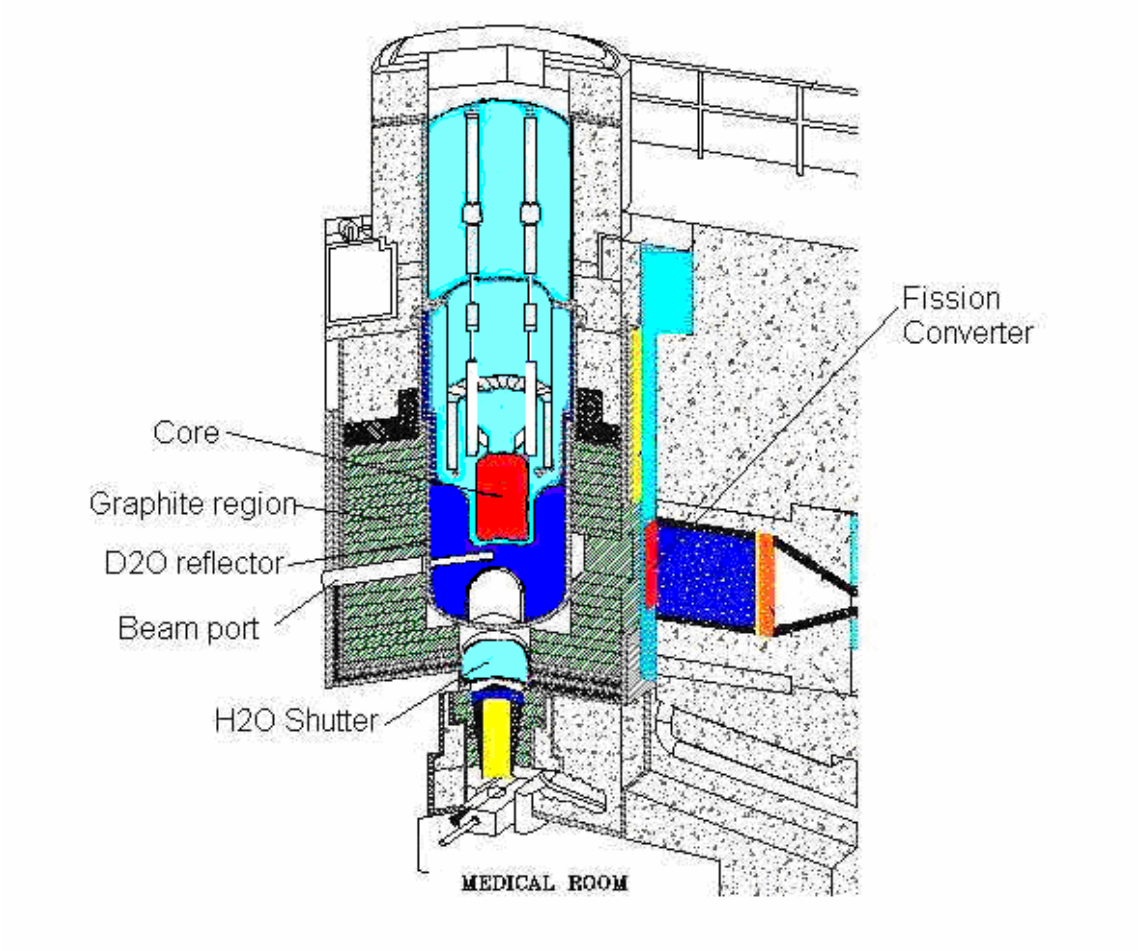

Figure 2-4. Overview of MITR-II reactor and facilities.

2.2 Core Geometry Description

Six control blades surround the core to shutdown the reactor at any time. In addition, the D_2O reflector can be dumped in order to provide a secondary means of reactor shutdown. The safety blades are made of 304 stainless steel impregnated with boron. Each safety blade can be controlled independently, but the set of six blades is typically banked for normal operation. When in the inserted position their bottoms are 10.25 inches below the reactor median plane. When they are moved 21 inches along their axes to the withdrawn position, their bottoms are 10.75 inches above the reactor median plane.

The MITR-II HEU fuel element is rhomboid-shaped with fifteen flat plates swaged to two side plates, as shown in Figure 2-5 and Figure 2-6 [2]. The plates are swaged to the two side plates which are welded to end fittings on the top and bottom. Once assembled, the fuel element is 2.375 inches external dimension (from outer edge of one side plate to the outer edge of the other side plate), and is a rhomboid with a 30º angle. Each element is 26.25 inches long including the end caps.

Each aluminum-clad fuel plate consists of 6061 Al alloy and a fuel meat core using HEU (93.15% enriched) in a dispersion of UAlx aluminide cermet in an aluminum matrix with a fuel thickness of 0.030 inches and a length of 23 inches. The extent of the meat is 22.375 inches long by 2.082 inches wide in each plate. In addition to a 0.015 inch thick solid cladding, each fuel plate has 0.010 inch fins to increase heat transfer to the coolant. Modeling of the HEU clad in MCNP is done by preserving the aluminum present, but without modeling of fin detail. Thus, the 0.010 inch square fins, spaced 0.010 inches from one another, are modeled as a part of a single planar clad 0.020 inches thick.

A proposed MITR-II LEU fuel element fueled with U10Mo, as described in Chapter 3, would have exterior element dimensions identical to HEU geometry except the LEU element would consist of 18 fuel plates with 0.020 inch thick fuel, and 0.010 inch thick cladding with 0.010 inch fins [3]. Whether these smaller dimensions will be feasible depends on several factors including intrinsic fuel properties and how these interact with manufacturing methods used in the fabrication.

HEU elements currently used in the core nominally contain 508 g ^{235}U each [4]. The material compositions of various historic HEU, and proposed LEU, fuel elements modeled in this report are discussed in Chapter 3.

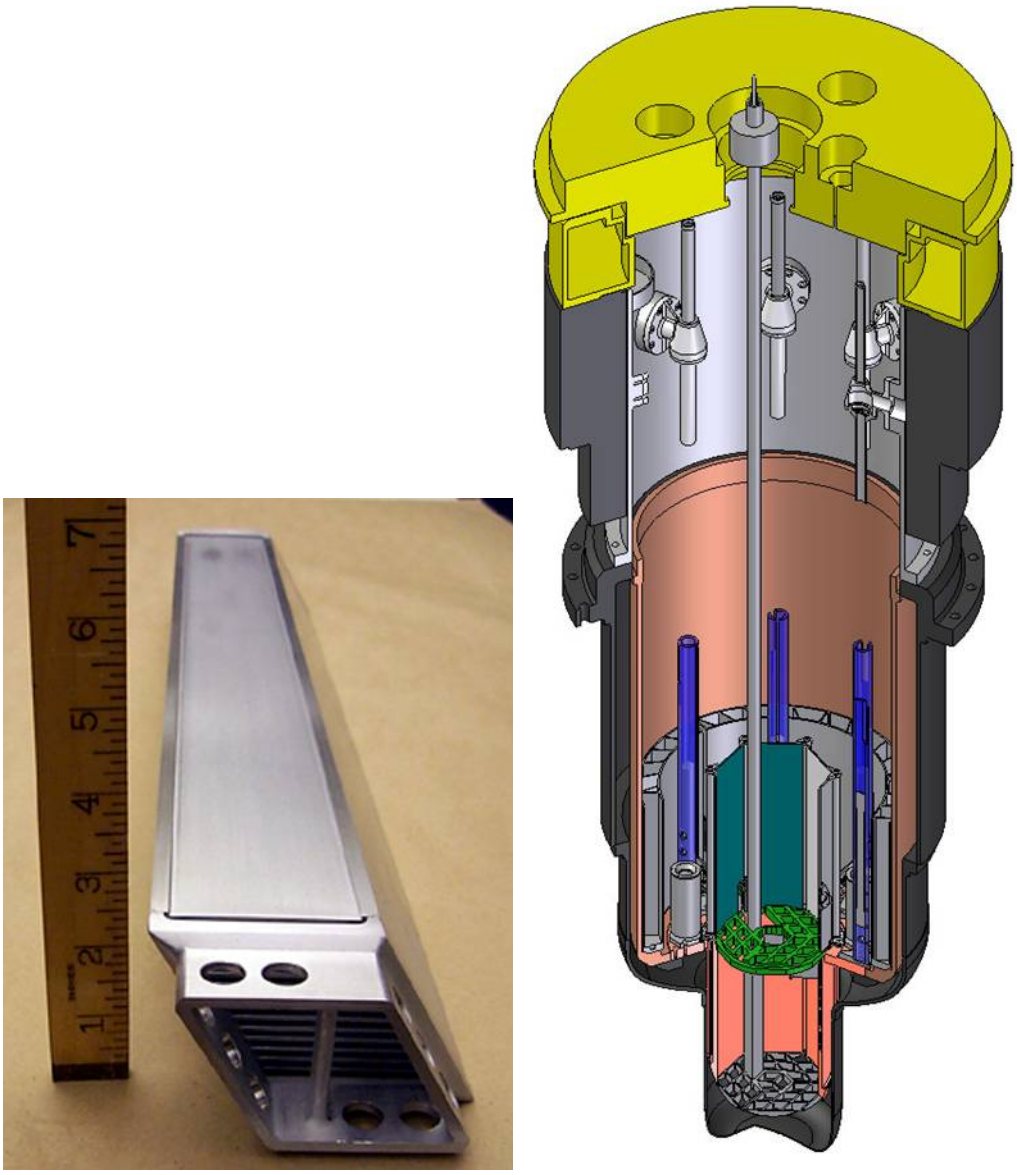

Figure 2-5. Reactor fuel element, at left. At right, cross section of the reactor being fueled with one element.

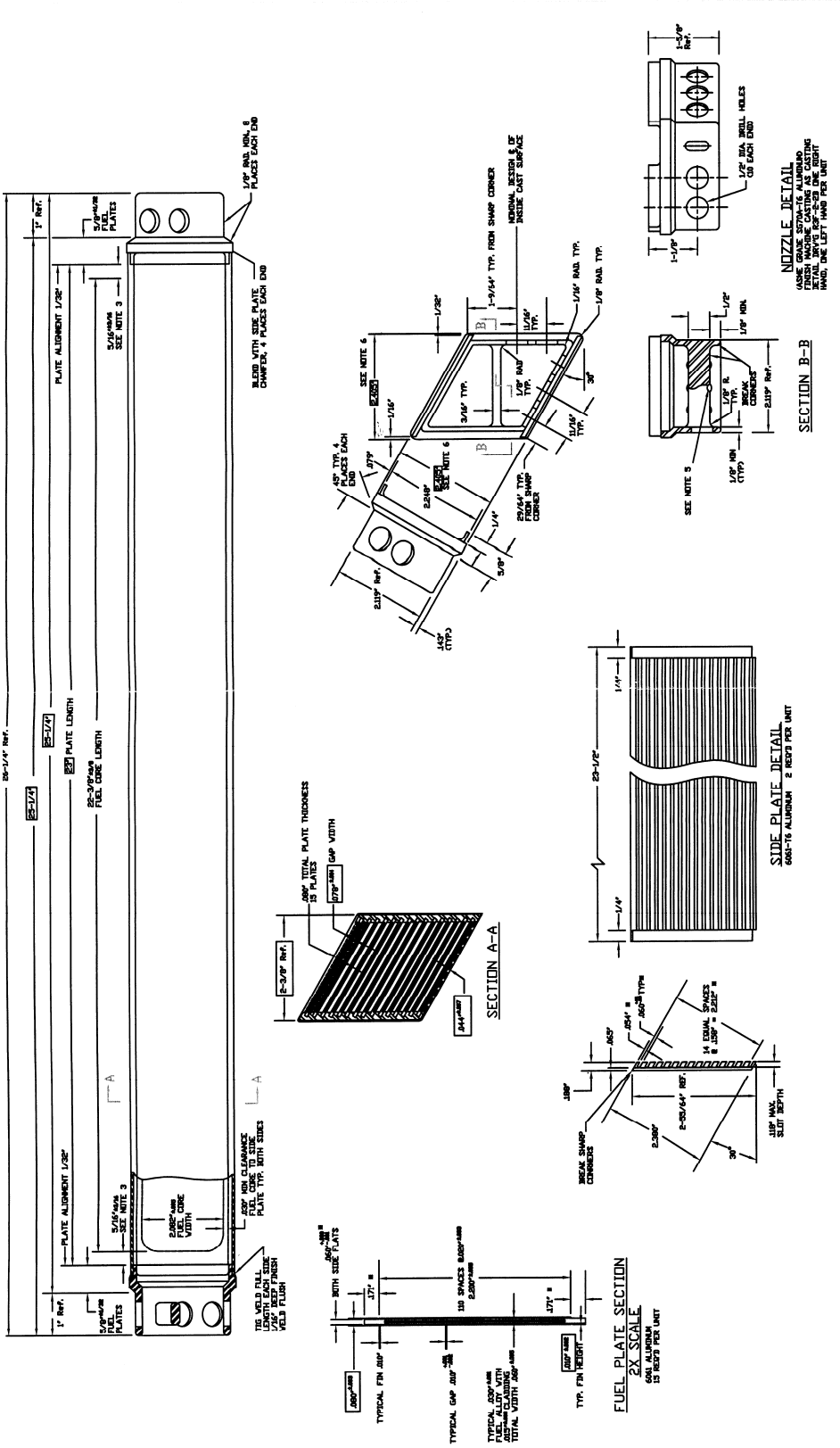

Figure 2-6. MITR-II HEU fuel element drawing.

2.3 Core Configuration and Fuel Loading

Various core configurations were modeled in this report in order to provide a capability to model a variety of scenarios for calculations of prior experiments. The core loading pattern for each of these cores in presented in the following sections. Core fuel element loadings are described in this report by the locations of the non-fuel dummy elements following the conventional MITR-II designations as shown in Figure 2-7 [1]. Details of other core modifications can be found in the discussion of the historical cores in section 4.1.1.

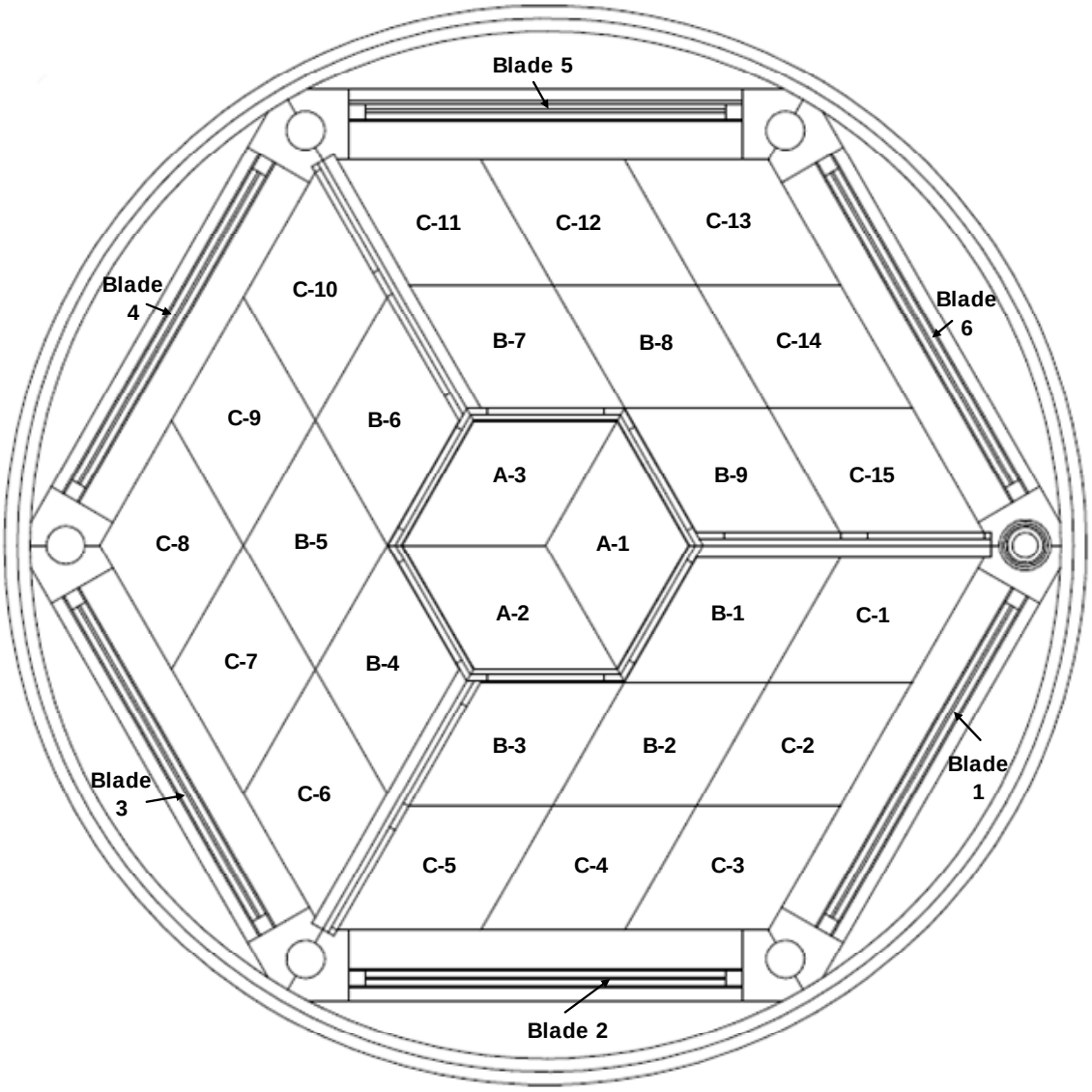

Figure 2-7. General core loading location designations for MITR-II.

This figure also labels the designations of the six control blades which are identical in design and located at the same radial distance from the core center. The blades are distinguished from one another in the calculations made for this report as follows: as viewed from the top of the reactor, control blade #1 is the first blade clockwise from the regulating rod, and blade #2 is the next blade clockwise, so that blade #6 is opposite the regulating rod from control blade #1. This report follows the MITR-II designations so that experimental blade numbering is presented consistently with calculations in this report.

2.3.1 Core 1 Configuration

The core loading configuration of core 1 consisted of 24 fuel elements loaded into the MITR-II core so that non-fuel dummy elements were present in the B2 and B8 locations, and an In-Core Sample Assembly (ICSA) was present in location A1 [5]. Fixed absorbers of cadmium were also present in the upper spider assembly. As viewed from the top, with the regulating rod at right, Figure 2-8 shows the modeled core loading for core 1.

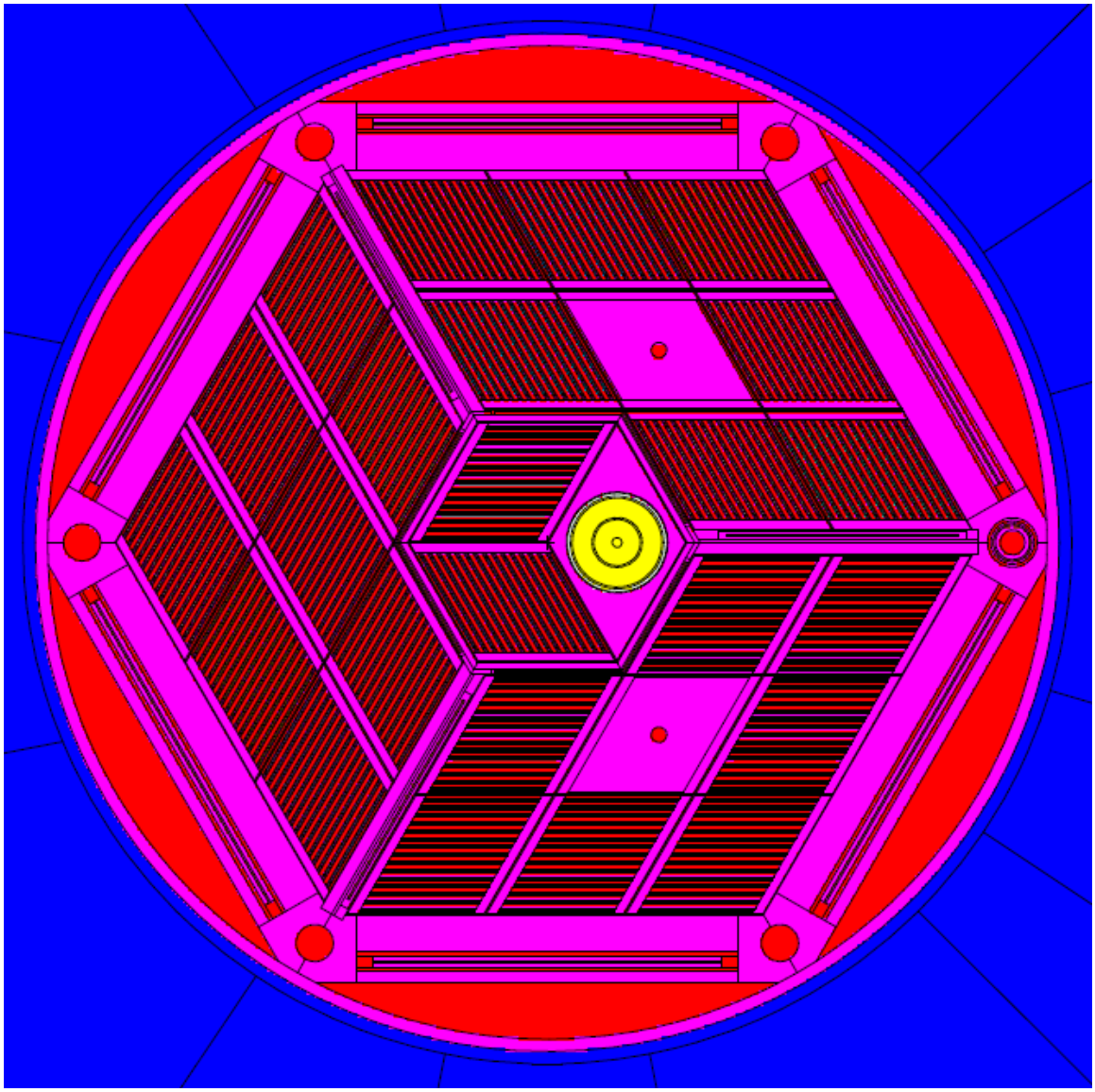

Figure 2-8. Core 1 fuel loading and configuration.

2.3.2 Core 2 Configuration

The core loading configuration of core 2 consisted of 22 fuel elements loaded into the MITR-II core so that non-fuel dummy elements were present in the A2 A3 B3 B6 and B9 locations, with no fixed absorbers [5] [6]. As viewed from the top, with the regulating rod at right, Figure 2-9 shows the modeled core loading for core 2.

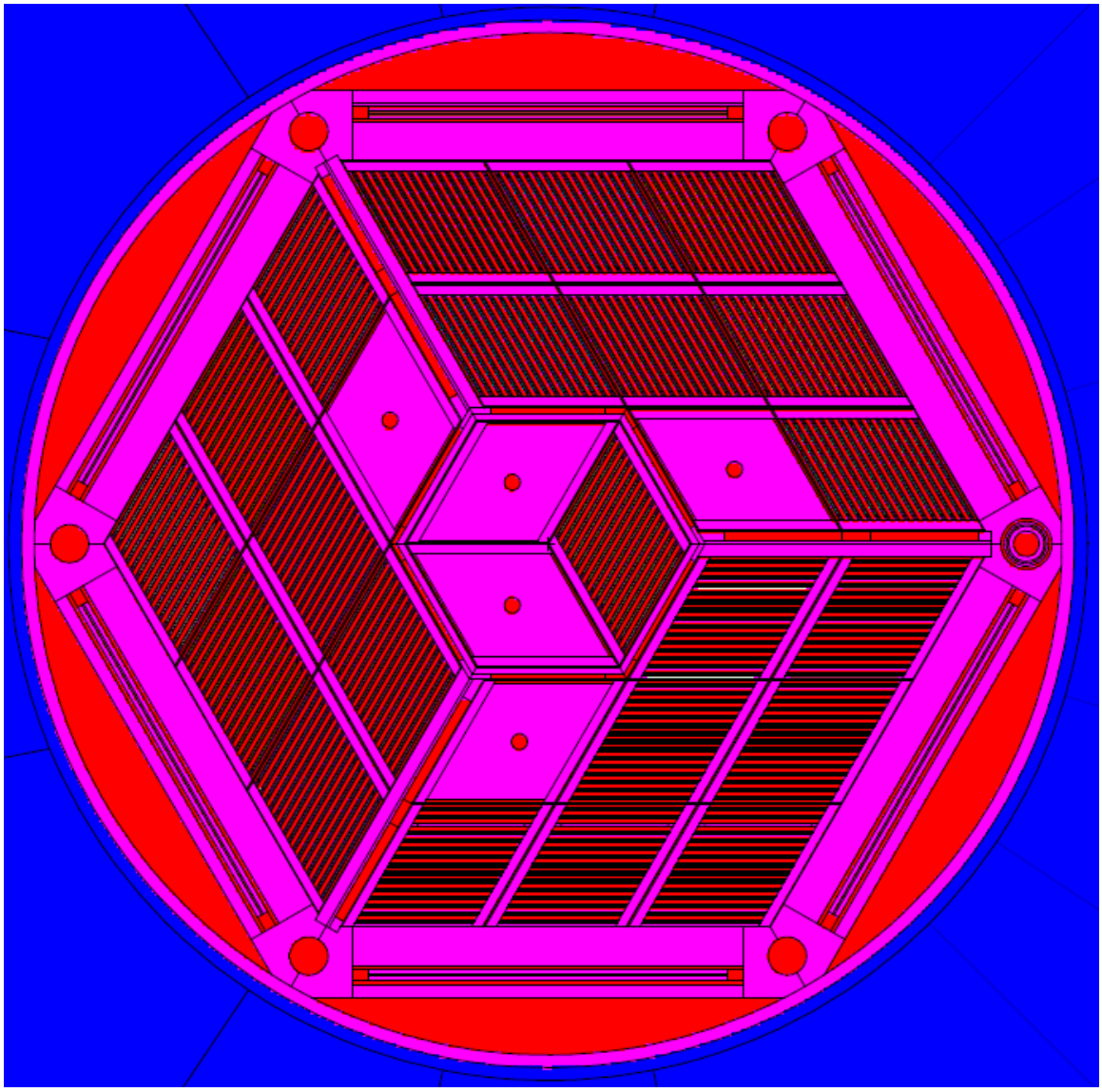

Figure 2-9. Core 2 fuel loading and configuration.

2.3.3 Core 4 Configuration

The core loading configuration consisted of core 4 consisted of 23 fuel elements loaded into the MITR-II core so that non-fuel dummy elements were present in the A1 A3 B2 and B4 locations [5]. The fuel element present in the B2 location during core 2 was moved to the B9 location for core 4. Three very low burnup elements, which were assumed to be fresh, were added into the A2 B3 and B6 locations. As viewed from the top, with the regulating rod at right, Figure 2-10 shows the modeled core loading for core 4.

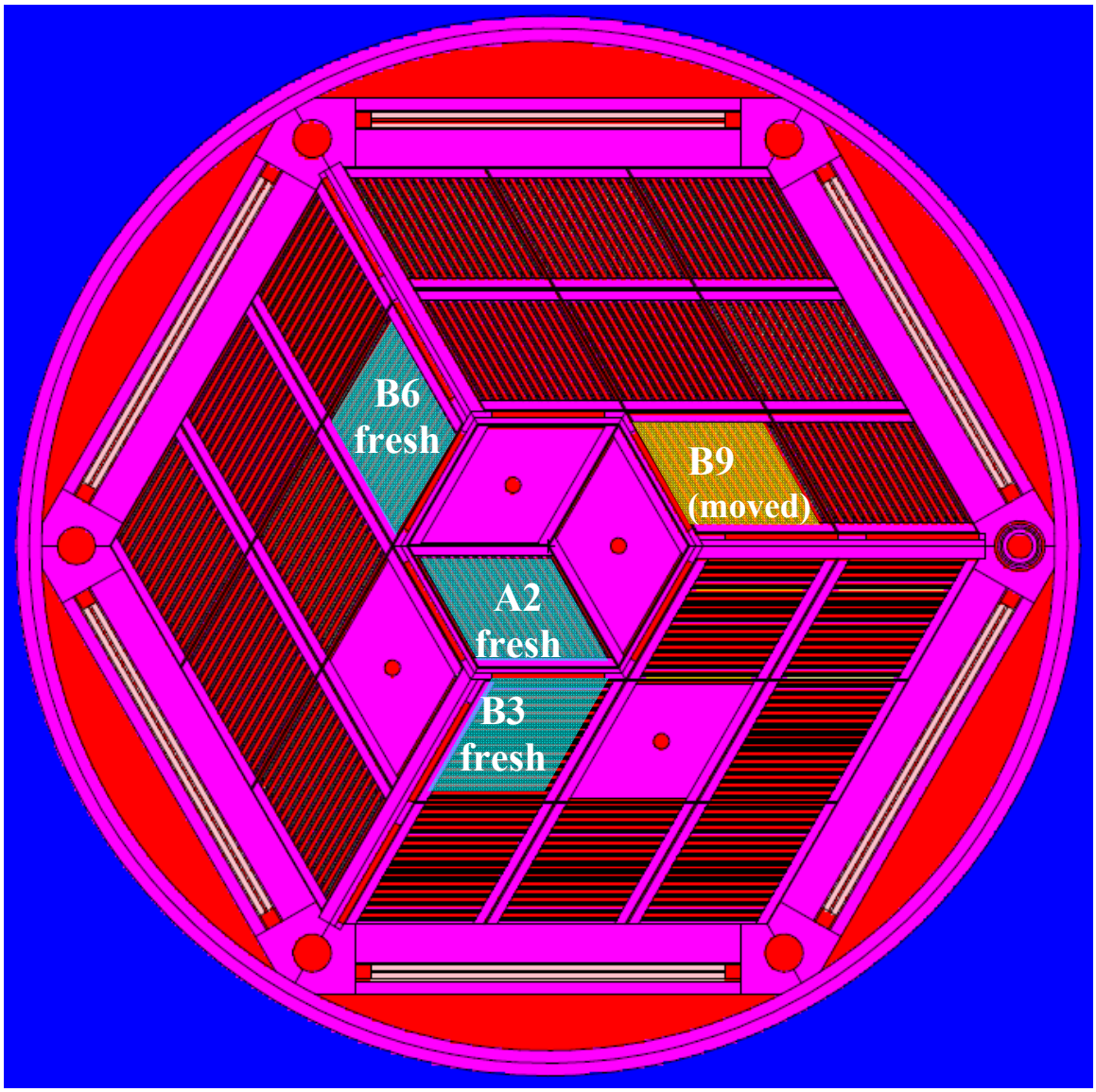

Figure 2-10. Core 4 fuel loading and configuration.

2.3.4 Core 180-188 Configuration

The core loading configuration of cores 180-188 consisted of 24 fuel elements loaded into the MITR-II core so that non-fuel dummy elements were present in the A1 A3 and B3 locations. Fuel shuffling of new and depleted elements was performed according to the records presented in Table 5-1. As viewed from the top, with the regulating rod at right, Figure 2-11 shows the modeled core loading for cores 180-188.

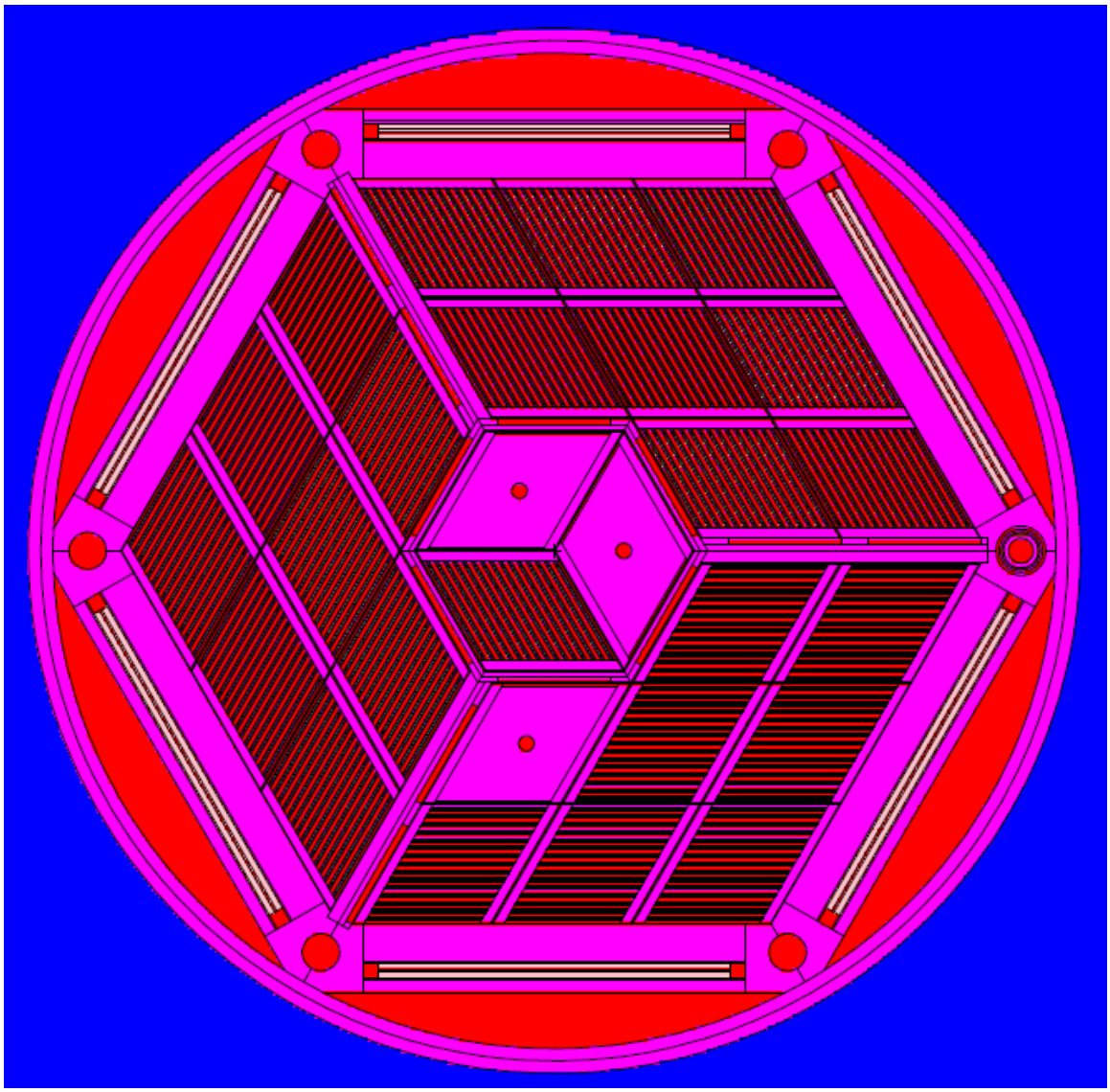

Figure 2-11. Core 180-188 fuel loading and configuration.

2.3.5 Core 179, 189 and 190 Configuration with ACI sample assembly

The core loading configuration of cores 179, 189 and 190 consisted of 24 fuel elements loaded into the MITR-II core following the pattern of fuel loading presented in Table 5-1 so that non-fuel dummy elements were present in the A1 and A3 locations, and the ACI experimental assembly was present in location B3. Fuel shuffling of new and depleted elements was performed according to the records presented in Table 5-1. As viewed from the top, with the regulating rod at right, Figure 2-12 shows the modeled core loading for cores 179, 189 and 190.

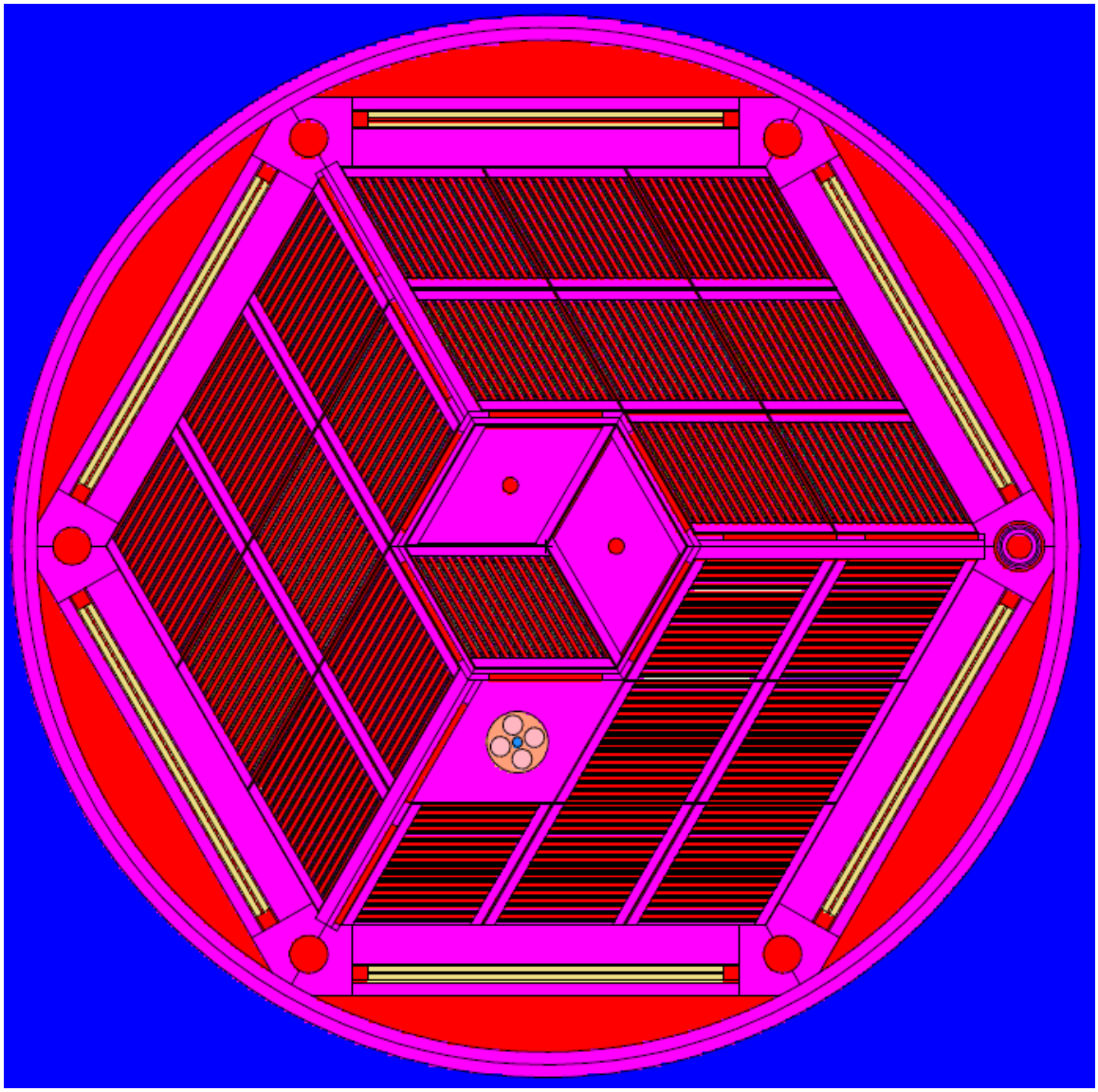

Figure 2-12. Core 179, 189 and 190 fuel loading and configuration with ACI assembly.

2.3.6 LEU Core Configuration

The core loading configuration of the LEU core, like HEU core 2, consisted of 22 fuel elements loaded into the MITR-II core so that non-fuel dummy elements were present in the A2 A3 B3 B6 and B9 locations. As viewed from the top, with the regulating rod at right, Figure 2-13 shows the modeled core loading for the fresh LEU core which served as the basis for calculations in this report. This fuel configuration was chosen as the basis for LEU studies of an all-fresh core since a core with a minimum of five dummies was required to satisfy the shutdown margin requirement, as discussed in section 4.4.4. The specific locations of the non-fuel dummy elements were chosen to match the dummy locations of core 2, which was similarly a (nearly) fresh core with 5 dummy elements. Note that although core 2 and the LEU core studied share the same fuel loading configuration, all other aspects of LEU core internals and control match the most recent core modeled, namely core 190, as summarized in Table 4-1.

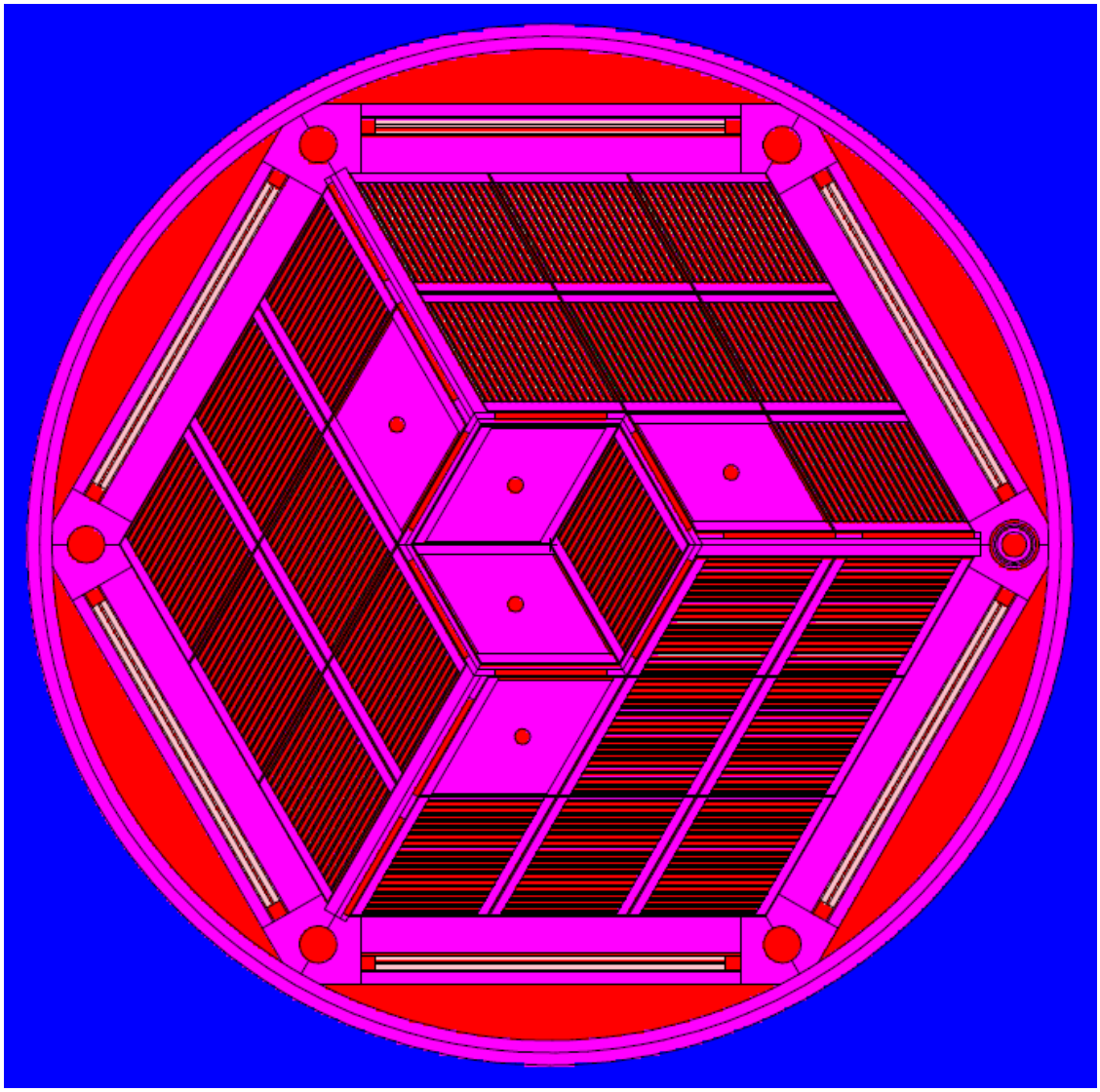

Figure 2-13. LEU core fuel loading and configuration.

3 Material Definitions in HEU and LEU Models

The material definitions used in various HEU and LEU core models are presented below. Where a material is presented, the density, mass fraction, and atomic density is given for each isotope. All calculations presented in this report have been defined with ENDF/B-VII libraries for individual isotopes, except for carbon which used the only available ENDF/B-VII library in natural abundance, and the definition of the ACI ICSA which was limited to a few historical core comparisons. Unless a calculation required a temperature change, and noted the use of a different library, the ENDF/B-VII 20.46ºC cross-section library and ENDF/B-VII 20.46ºC S(α,β) libraries were used. S(α,β) libraries were applied to graphite, and all materials containing light and heavy water.

3.1 Fuel

3.1.1 HEU Fuel

Several different vendors have been used to supply HEU fuel elements for use in the MITR-II reactor. A brief overview of the MITR-II fuel history is given in references [1] and [7]. This section describes the material definition used to model fuel used in the start-up phase, as well as the fuel currently used in the MITR-II reactor.

3.1.1.1 HEU Fuel during the time of 1975 Start-up

The initial fuel loaded into the MITR-II reactor during the fresh fuel start-up in 1975 used uranium enriched to 93.15% ^{235}U with 445 g ^{235}U per element, and is modeled using the composition and density shown in Table 3-1[8] [9].

Table 3-1. Isotopic description of the HEU 445 g ^{235}U element fuel as used in modeling.

Nuclide	Density (g/cm^3)	Mass fraction (^{wt}%)	Atom density (barn^{-1}cm^{-1})
^{27}Al	2.2597	61.904%	5.0435E-02
^{234}U	0.0142	0.390%	3.6585E-05
^{235}U	1.2954	35.487%	3.3190E-03
^{236}U	0.0047	0.127%	1.1865E-05
^{238}U	0.0764	2.093%	1.9324E-04
Total	**3.6504**	**100%**	**5.3995E-02**

3.1.1.2 Modern HEU Fuel used for cores 178 - 190

The fuel currently in use is provided by Babcock & Wilcox Co. This is the only fuel type loaded into the core during the series of modeled cores 178 to 190 which operated over the time period from 2007 to 2009. Current fuel uses uranium enriched to 93.15% ^{235}U with 508 g ^{235}U per element, and is modeled using the composition and density shown in Table 3-2 [8] [9]. These values were derived based on the nominal ^{235}U loading of 508 grams [4].

Table 3-2. Isotopic description of the HEU 508 g ^{235}U element fuel as used in modeling.

Nuclide	Density (g/cm^3)	Mass fraction (^{wt}%)	Atom density (barn^{-1}cm^{-1})
^{27}Al	2.2241	58.351%	4.9640E-02
^{234}U	0.0162	0.426%	4.1771E-05
^{235}U	1.4788	38.796%	3.7888E-03
^{236}U	0.0053	0.139%	1.3546E-05
^{238}U	0.0872	2.288%	2.2060E-04
Total	**3.8117**	**100%**	**5.3705E-02**

3.1.2 Proposed LEU Fuel

The proposed LEU fuel for use in the MITR-II reactor is based on a monolithic alloy fabrication technology, which is currently in the qualification phase of development. This section presents the best known assumptions for a constituent uranium-molybdenum monolithic alloy enriched up to 19.75% ^{235}U, in the form presently recommended with 10^{wt}% Mo [10]. The composition of the fuel used in the MCNP modeling is presented in Table 3-3.

Table 3-3. Isotopic description of the LEU U10Mo fuel as used in modeling.

Nuclide	Density (g/cm^3)	Mass fraction (^{wt}%)	Atom density (barn^{-1}cm^{-1})
^{92}Mo	0.2408	1.415%	1.5775E-03
^{94}Mo	0.1538	0.903%	9.8567E-04
^{95}Mo	0.2677	1.573%	1.6986E-03
^{96}Mo	0.2838	1.667%	1.7812E-03
^{97}Mo	0.1644	0.966%	1.0213E-03
^{98}Mo	0.4202	2.469%	2.5844E-03
^{100}Mo	0.1714	1.007%	1.0326E-03
^{234}U	0.0398	0.234%	1.0248E-04
^{235}U	3.0253	17.775%	7.7513E-03
^{236}U	0.0705	0.414%	1.7977E-04
^{238}U	12.1824	71.577%	3.0819E-02
Total	**17.0200**	**100%**	**4.9534E-02**

Because the UMo fuel is still under qualification, it is difficult to predict the manufacturing uncertainties in fabrication, including mean and statistical distributions in density. The fuel defined in Table 3-3 is based on a UMo fuel containing 10^{wt}% molybdenum having a theoretical density of 17.7 g/cm^3 [11] and accounting for an approximate 1% porosity [12] in the fuel resulting in a modeled density of 17.02 g/cm^3. The geometry of the LEU fuel element, as discussed in Chapter 2, and this LEU composition yield an element modeled with 831.4 g of ^{235}U. Note that this represents an increase of 323.4 g ^{235}U per element relative to the current HEU (i.e., a 64% increase in ^{235}U per element). The mass of U per element increases to 4.2 kg for an LEU element. Compared to the 0.55 kg U per HEU element, this is an increase of 3.65 kg U per element (i.e., a 664% increase in U per element). The total mass of the element including fuel meat, cladding, side plates and end fittings is thus expected to increase to 7.2 kg. This is an 81% increase compared to the modeled HEU element mass of 4.0 kg.

3.2 Control Materials

3.2.1 Cadmium Control Material

Cadmium (Cd) is defined in the model for three purposes. First, it was used as a fixed absorber by attaching six aluminum-clad Cd plates to the internal structure within the array of fuel elements during core 1. A Cd plate was attached to each of the three radial arms. The remaining three plates were bent so that they each covered two of the six outer faces of the hexagonal strut.

Second, Cd was used as the control blade material for cores 1 and 2. Throughout the duration of core 2 the control blades were changed out, one at a time, to Borated Stainless Steel (BSS) blades, as described in subsequent sections of this report. Since core 2 startup experiments were performed at the beginning of core 2, Cd blades are in place for all experimental and calculated results presented in this report for core 2.

Subsequent to core 2, the only Cd present in the core has been in the regulating rod. The Cd material is defined in all cases by a material of density 8.65 g/cm^3, and a composition of pure Cd with the isotopic definition found in Table 3-4.

Table 3-4. Cadmium control material definition.

Nuclide	Density (g/cm^3)	Mass fraction (^{wt}%)	Atom density (barn^{-1}cm^{-1})
^{106}Cd	0.1019	1.178%	5.7924E-04
^{108}Cd	0.0739	0.854%	4.1242E-04
^{110}Cd	1.0563	12.211%	5.7878E-03
^{111}Cd	1.0924	12.628%	5.9314E-03
^{112}Cd	2.0778	24.021%	1.1182E-02
^{113}Cd	1.0617	12.274%	5.6627E-03
^{114}Cd	2.5181	29.111%	1.3313E-02
^{116}Cd	0.6680	7.723%	3.4708E-03
Total	**8.6500**	**100%**	**4.6339E-02**

3.2.2 Control Blade with Nominal Boron Content

Whereas the nominal value of the boron in the control blades has been cited as 1^{wt}% B and 1.1^{wt}% B in references [1] and [5], respectively, the MCNP model definition for the historical cores has been left at 1.06^{wt}% B as found in other work [7]. Table 3-5 gives the material definition used in the MCNP model for all cores with borated blades presumed to contain a nominal boron content of 1.06^{wt}%. In this report, HEU core 4 and the LEU core were modeled with a nominal boron content of 1.06^{wt}%.

Table 3-5. Control Blade material definition for a typical core with 1.06^{wt}% B.

Nuclide	Density (g/cm^3)	Mass fraction (^{wt}%)	Atom density ($barn^{-1}cm^{-1}$)
^{10}B	0.0157	0.195%	9.4334E-04
^{11}B	0.0694	0.865%	3.7963E-03
C	0.0032	0.040%	1.6099E-04
^{28}Si	0.0472	0.588%	1.0160E-03
^{29}Si	0.0025	0.031%	5.1587E-05
^{30}Si	0.0017	0.021%	3.4007E-05
^{31}P	0.0009	0.011%	1.7167E-05
^{32}S	0.0003	0.004%	6.0302E-06
^{50}Cr	0.0620	0.773%	7.4774E-04
^{52}Cr	1.2436	15.493%	1.4419E-02
^{53}Cr	0.1437	1.791%	1.6349E-03
^{54}Cr	0.0364	0.454%	4.0693E-04
^{55}Mn	0.1300	1.620%	1.4254E-03
^{54}Fe	0.2916	3.633%	3.2555E-03
^{56}Fe	4.7468	59.134%	5.1105E-02
^{57}Fe	0.1116	1.390%	1.1803E-03
^{58}Fe	0.0151	0.188%	1.5701E-04
^{58}Ni	0.7428	9.253%	7.7206E-03
^{60}Ni	0.2960	3.687%	2.9740E-03
^{61}Ni	0.0131	0.163%	1.2928E-04
^{62}Ni	0.0424	0.528%	4.1219E-04
^{64}Ni	0.0111	0.139%	1.0497E-04
Total	**8.0272**	**100%**	**9.1698E-02**

3.2.3 Control Blade with Boron Content per Analysis

During the definition of the model, the compositional analysis of the particular lot of 304B4 grade B stainless steel used to fabricate the control blades in a 2001 order was obtained, as shown in Table 3-6 [13], and implemented into the MCNP model only for cores 178-190. The control blade analyzed contained $1.29^{wt}\%$ boron with an isotopic ratio of ^{10}B $19.9\%_{atom}$ and ^{11}B $80.1\%_{atom}$. Trace elements were also present in the compositional analysis, and were included in the material definition of cores 178-190 MCNP control blade material definition as shown in Table 3-7. Substantial changes are present, and the 22% difference in B atom density is of significant neutronic importance.

Table 3-6. Borated stainless steel control blade composition for cores 178-190.

Ladle analysis of 304B4 SS material in 2001 shipment of borated steel control blades								
Element	**C**	**Mn**	**S**	**Si**	**Cr**	**Ni**	**P**	**B***
Analysis wt%	0.012%	0.57%	0.001%	0.40%	18.77%	12.48%	0.02%	1.29%

*Analysis isotope ratio determination: ^{10}B ($\%_{atom}$) = 19.9
^{11}B ($\%_{atom}$) = 80.1

Table 3-7. Control Blade material definition for cores 178-190 per the 1.29^{wt}% B ladle analysis.

Nuclide	Density (g/cm^3)	Mass fraction (^{wt}%)	Atom density (barn^{-1}cm^{-1})
^{10}B	0.0191	0.238%	1.1479E-03
^{11}B	0.0845	1.052%	4.6202E-03
C	0.0010	0.012%	4.8297E-05
^{28}Si	0.0295	0.367%	6.3497E-04
^{29}Si	0.0016	0.019%	3.2242E-05
^{30}Si	0.0011	0.013%	2.1254E-05
^{31}P	0.0016	0.020%	3.1213E-05
^{32}S	0.0001	0.001%	1.5076E-06
^{50}Cr	0.0629	0.783%	7.5824E-04
^{52}Cr	1.2611	15.710%	1.4621E-02
^{53}Cr	0.1457	1.816%	1.6579E-03
^{54}Cr	0.0370	0.460%	4.1264E-04
^{55}Mn	0.0458	0.570%	5.0154E-04
^{54}Fe	0.3012	3.752%	3.3624E-03
^{56}Fe	4.9026	61.075%	5.2782E-02
^{57}Fe	0.1153	1.436%	1.2190E-03
^{58}Fe	0.0156	0.194%	1.6217E-04
^{58}Ni	0.6732	8.386%	6.9973E-03
^{60}Ni	0.2682	3.342%	2.6953E-03
^{61}Ni	0.0119	0.148%	1.1716E-04
^{62}Ni	0.0384	0.479%	3.7357E-04
^{64}Ni	0.0101	0.126%	9.5138E-05
Total	**8.0272**	**100%**	**9.2294E-02**

3.2.4 Depleted Borated Stainless Steel Fixed Absorber Inserts

MITR-II currently has installed six 5-inch long fixed absorbers in the 3 radial arms which are composed of (depleted) borated stainless steel. Complete depletion is assumed as these inserts have not been removed from the reactor over the course of several decades of operation. Thus the same material definition used for the control blade with nominal boron content in Section 3.2.2 of this report has been used for the depleted steel inserts with the exception that all ^{10}B has been depleted.

3.3 Moderator and Reflector

Throughout the course of benchmark comparisons for a wide variety of experiments, the light water (H_2O) moderator and D_2O reflector were modified appropriately in terms of densities, and temperature. Where experiments specified a fluid temperature, the NIST database of material properties was used to provide fluid densities, at atmospheric pressure, which were inserted into the model [14]. Atmospheric pressure was modeled since the pool extends 10 feet above the core outlet. The 1 to 2 atmospheres of pressure present in the reactor would alter the density negligibly (<0.005%). Where required to calculate specific temperature coefficients of reactivity, as in the case of isothermal measurements, the S(α,β) cross-section library temperature was modified in addition to densities. However the small range of temperatures for steady-state analyses in this report did not require any changes from room temperature cross-section libraries, other than the cases explicitly indicated in this report.

Most experiments were performed at an isothermal moderator and reflector temperature of 25°C at or near zero power to prevent Xe and temperature reactivity swings. For calculations at other temperatures, effects were taken into account by a change of density and tmp card entry in MCNP. The water temperature for all calculations presented in this report is 25°C unless otherwise specified. Table 3-8 presents the density of light and heavy water used in the models.

Table 3-8. Water densities used in calculations at various temperatures.

Case	H2O temperature (ºC)	H2O density (g/cm^3)	D2O temperature (ºC)	D2O density (g/cm^3)
Shutdown margin calculation	10.00	0.999702	10	1.10601
S(α,β) .10t library temperature	20.46	0.998111	20.46	1.10532
S(α,β) .11t library temperature	76.85	0.973722	76.85	1.08028
Typical experimental condition (25ºC)	25.00	0.997048	25.00	1.10450
HEU inlet H2O (5 MW nominal full power)	44.00	0.990628	-	-
HEU mixed mean H2O (5 MW nominal full power)	48.00	0.988926	-	-
Heavy water (5 MW nominal full power)	-	-	54.00	1.09374

For cores 178 – 190 that were depleted, all calculations were assumed to be at the nominal full-power (which was 5 MW at the time) temperature and density for the reactor. Water in the active portion of the core was set at the mixed mean temperature of 48°C (since 5 MW operation yields a 44°C inlet and 52°C outlet temperature) and the remaining light water at the 44°C inlet temperature. For the depletions at power, heavy water in the reflector was set to reflect normal operation with a density and temperature corresponding to 54°C.

3.4 Aluminum Alloy

The aluminum alloy used in the cladding and other aluminum structural materials in the reactor is 6061 aluminum with the constituent elements listed in Table 3-9. The impact of trace boron impurities, which may be present in modern 6061 aluminum, was evaluated. However, since this was found to have negligible impact, boron was not included in the composition of the aluminum alloy.

Table 3-9. Isotopic description of the 6061 Al alloy fuel as used in modeling.

Nuclide	Density (g/cm^3)	Mass fraction (^{wt}%)	Atom density (barn^{-1}cm^{-1})
^{24}Mg	0.0211	0.781%	5.3098E-04
^{25}Mg	0.0028	0.103%	6.7240E-05
^{26}Mg	0.0032	0.118%	7.3976E-05
^{27}Al	2.6239	96.869%	5.8563E-02
^{28}Si	0.0150	0.552%	3.2188E-04
^{29}Si	0.0008	0.029%	1.6344E-05
^{30}Si	0.0005	0.020%	1.0774E-05
^{46}Ti	0.0003	0.012%	4.2202E-06
^{47}Ti	0.0003	0.011%	3.8048E-06
^{48}Ti	0.0030	0.111%	3.7715E-05
^{49}Ti	0.0002	0.008%	2.7672E-06
^{50}Ti	0.0002	0.008%	2.6526E-06
^{50}Cr	0.0003	0.010%	3.4262E-06
^{52}Cr	0.0057	0.210%	6.6068E-05
^{53}Cr	0.0007	0.024%	7.4912E-06
^{54}Cr	0.0002	0.006%	1.8646E-06
^{55}Mn	0.0041	0.150%	4.4610E-05
^{54}Fe	0.0011	0.040%	1.1971E-05
^{56}Fe	0.0175	0.644%	1.8791E-04
^{57}Fe	0.0004	0.015%	4.3399E-06
^{58}Fe	0.0001	0.002%	5.7733E-07
^{63}Cu	0.0051	0.189%	4.8906E-05
^{65}Cu	0.0023	0.087%	2.1794E-05
Total	**2.7087**	**100%**	**6.0034E-02**

4 Comparison of Model Results to Experimental Start-up Benchmark Data

4.1 Overview of Experimental Benchmark Data

A variety of sources exist for MITR-II experimental measurements of reactor physics parameters. In addition to information in the Safety Analysis Report [1], there is a large collection of start-up information and data collected. A general history of particular interest is contained in two documents: "The Reactor Engineering of the MITR-II Construction and Startup" [15], and the "MITR-II Start-up Report" [5]. It is the latter of these which contains the majority of measured data cited in this report. Additionally, the authors have chosen to present several records of experimental measurements from MITR-II archival log entries which may not previously have been made available in a report. This has been done to present as complete a set of measurements as is presently available across the history of MITR-II reactor configurations. This breadth enables analyses towards the conversion from HEU to LEU fuel. The start-up data serves a two-fold purpose. Firstly, the start-up data provides the basis of operation in the MITR HEU SAR [1] with the majority of data cited directly from the MITR-II Start-up Report [5]. Secondly, benchmarking of the MCNP model to experimental data is highly desirable for verification and validation purposes. Whereas previous comparisons to historical start-up reference data for undepleted cores had been performed, agreement between modeled and experimental conditions was varied and included discrepancies in predicted reactivity $\geq 1\%$ [7] for representative cores. While this chapter deals with start-up data on fresh, or nearly fresh historical cores 1 through 4, chapter 5 of this report will address benchmarks on depleted cores in recent MITR-II history.

4.1.1 Historical start-up cores

As summarized in Table 4-1, the MITR-II reactor underwent many changes to core configuration, core internal structure, fuel composition, and movable and fixed absorber reactivity control devices between the first core and present. All of the core configurations listed have been constructed with models representing specifications of reactor design with the exception of core 3. Core 3 included hafnium inserts in the spider (where the term spider refers collectively to the hexagonal strut and three connected radial arms), and never operated above low power. Core 3 was not modeled because it operated for a short time with limited collection of data. MITR-II has never again been operated with hafnium. Regarding the changes in geometry from core to core, a series of specification drawings have been used. These include drawings for the original upper spider [16], and modern upper spider [17], cadmium [18] and borated stainless steel [19] [20] [21] control blades, and fixed absorber inserts made of Cd [22], hafnium [23], and BSS [24]. Also, specification drawings which did not vary among any of these cores were incorporated into the model. These included the fuel element [2], lower spider [25],

solid non-fuel dummy element with cooling hole [26], regulating rod [27], core housing-housing body [28], core housing lower grid plate [29], and core tank-core housing assembly [30]. These formed the basis whereby MITR-II model geometry has been verified, and updated as required during the course of validation to represent the specifications of the MITR-II reactor as discussed in [31].

For convenience, fresh HEU fuel was used to model cores 1 and 2. This choice is justified by the very low burnup level during the low-power testing prior to high-power operation of these cores. In contrast the burnup at the beginning of core 4 is very significant, such that if fresh undepleted fuel were assumed, then the excess reactivity modeled for experimental criticals would be +2%. In order to account for burnup during core 4, a depletion history which approximates the operation to core 4 has been performed using REBUS-MCNP [32]. In this model the burn-up and shuffling have been modeled as summarized in Table 4-1.

Since a detailed depletion using records of operation at various reactor powers is beyond the scope of this study, a simplified operation history was adopted. The reactor operation for 568 MWh during core 1 was combined with the core 2 reactor operation for 5520 MWh so that a depletion assumed a simplified operation in a core 2 configuration for 102 days at 2.5 MW with the core BOC critical blade height of 8.3 inches. A power of 2.5 MW was chosen since this was the half power level up to which MITR-II ran prior to ramping up to full power (5 MW at that time) during core 4 [5]. Fuel elements were shuffled between core 2 and core 4 such that the B2 core element was moved to the B9 location. The three elements added into the A2 B3 and B6 locations for core 4 were assumed to be fresh fuel since they were not present for the entirety of core 1, and were not present at all in core 2.

Comparisons to benchmark experimental data from a variety of different types of experiments during the course of these four cores in 1975-1976 will now be presented. MITR HEU SAR content is derived mostly from fresh core measurements. LEU safety calculations can also be made in the same manner as HEU calculations which represent the experimental measurement. Thus, this chapter presents HEU experimental measurements alongside HEU and LEU calculations for fresh cores in a variety of configurations and perturbed states.

Table 4-1. MITR-II core configuration overview from start-up to present cores.

MITR-II Configurations	Core 1	Core 2	Core 3	Core 4	Cores 178-190
First critical date	Sept 8 1975	Mar 9 1976	Nov 9 76	Nov 17 76	2007-2009
Fuel elements	24	22	25	23	24
^{235}U per element	445 g	445 g	445 g	445 g	508 g
Non-fuel dummy elements Location	2 solid with hole B2 B8	5 solid with hole A2 A3 B3 B6 B9	2 solid with hole A1 A3	4 solid with hole A1 A3 B2 B4	3 solid with hole A1 A3 B3
Sample assemblies	2" ICSA in A1	0	0	0	ACI (varies)
Control blades	Cd	Cd *	**BSS**	**BSS**	**BSS**
Core internal spider, upper	original	original	**modern**	**modern**	**modern**
Upper spider absorbers	six Cd, nominal 10"above fuel bottom	none	twelve hafnium	none	six 5" depleted B-steel in arms
Spider, lower	original	original	original	original	original
Al flow shroud	no	no	**yes**	**yes**	**yes**
Critical height	7.36	8.6	7.72	7.3	various
Regulating rod	same assumed	same assumed	full-in	same assumed	see data
Fuel loaded	-	-	-	A2 B3 B6; partly core 1 depleted	see data
BOC burnup (MWd/kg HM)	fresh	2.1	-	22	partial refueling
Core operation (MW-days)	24.4	230.0	low power only	only BOC modeled	2327 over 12 cores

*Cadmium control blades present at the beginning of core 2 were replaced during the course of this core, one at a time, with stainless steel blades containing 1% nat. boron [5].

4.1.2 LEU core selection

The core configuration with 5 non-fuel dummy elements in the A2 A3 B3 B6 and B9 locations, as illustrated in section 2.3.6, was chosen as the basis for LEU calculations in this report. This configuration was selected since the all-fresh LEU core satisfied the shutdown margin requirement with a minimum of five dummies as discussed below in section 4.4.4. The specific locations of the non-fuel dummy elements were chosen to match the dummy locations of core 2, which was similarly a (nearly) fresh core with 5 dummy elements. This configuration had been the result of an optimization process performed during the loading of core 2, whereby the final configuration reduced the reactivity worth of the solid dummies and the power peaking in the vicinity of the water gaps created by removal of the absorbing inserts in the radial arms and hexagonal strut [5].

4.2 Comparison to Experimental Criticals

K-effective was modeled for the different HEU MITR-II configurations, core 1, core 2 and core 4. For each case, the Shim Bank (SB) and Regulating Rod (RR) were set at the first measured critical position. The LEU model has also been used to evaluate the k-effective. A search has been carried out to determine the critical position of the control elements. Table 4-2 presents the k-effective obtained by calculation for cores 1 to 4. Table 4-3 gives the control elements position which allows the LEU core to be critical.

Table 4-2. Calculated k-effective of core 1, core 2 and core 4 critical states.

HEU core	Core 1	Core 2	Core 4
Non-fueled element location	B2 B8 & ICSA in A1	A2 A3 B3 B6 B9	A1 A3 B2 B4
First critical control elements position (inches withdrawn)	7.36	8.3	7.3
First critical control elements position (cm withdrawn)	*18.6944*	*21.082*	*18.542*
Calculated k-effective	0.99700	1.00206	1.00420
Uncertainty 1-σ (pcm)	4	4	3
Deviation from critical (pcm)	-301	206	418

Table 4-3. Evaluated control elements position for critical LEU core.

Parameter	Critical LEU core
Non-fueled element location	A2 A3 B3 B6 B9
Calculated k-effective	1.00001
Uncertainty 1-σ (pcm)	3
Control elements position (inches withdrawn)	8.17
Control elements position (cm withdrawn)	*20.741*

Results obtained for core 1, core 2, and core 4 are in good agreement with experiment, where the bias is under 500 pcm in various core loading configurations which include both assumed-fresh and depleted fuel. Calculation shows that the LEU fresh core in the configuration with non-fueled elements in locations A2 A3 B3 B6 B9 is critical when the SB and RR control elements are set at 8.17 inches (20.741 cm exactly) withdrawn. Note that this critical position is very close to the core 2 critical position which has the same non-fueled element configuration. This is within the range of typical initial critical positions cited in the HEU SAR, where a typical range of 7 to 9 inches (17.78 to 22.86 cm) withdrawn is cited [1].

4.3 General Kinetic Parameters

HEU values for both the neutron lifetime and the effective delayed neutron fraction have been calculated and compared to LEU calculations. HEU calculations are compared to values cited in the MITR-II Start-up Report which were estimated prior to the modification in 1974-1975, where neutron lifetime was confirmed by both the dropped rod method and noise analysis as part of the startup testing [5]. In the MITR HEU SAR [1], the effective delayed neutron fraction cited is 0.00786. Table 4-4 compares the HEU and LEU effective delayed neutron fraction.

Table 4-4. Calculated effective delayed neutron fraction for LEU and HEU cores.

Core configuration	HEU core 1	HEU core 2	HEU core 4	LEU
Non-fuel dummy element location	B2 B8 ICSA in A1	A2 A3 B3 B6 B9	A1 A3 B2 B4	A2 A3 B3 B6 B9
Effective delayed neutron fraction *	0.00771	0.00769	0.00764	0.00761
Uncertainty 1-σ	0.00006	0.00006	0.00004	0.00004
Deviation from HEU reference value (%)	-2%	-2%	-4%	-3%

* The results do not include photoneutrons.

The effective delayed neutron fraction calculation does not include photoneutrons, and for the studied HEU fresh cores is consistently between 2%-4% below the reference value. A study of photoneutrons which included calculations of a fresh MITR reactor core cited a contribution to the effective delayed neutron fraction on the order of +1-2% for HEU and LEU MITR cores [33]. Although the calculated LEU effective delayed neutron fraction, 0.00761, is 1% lower than the calculated HEU value, 0.00769, all are in reasonable agreement given the uncertainties in the values, and the additional photoneutron contribution not included in this calculation.

Prompt neutron lifetime was calculated by the 1/v insertion method [34]. The measured prompt lifetime was 100 μs. The calculated prompt neutron lifetime of an LEU fueled fresh core is given in Table 4-5, along with the calculated HEU neutron lifetime. Both are significantly lower than the experimentally measured value of 100 μs. The LEU lifetime is significantly lower than the HEU calculation. However, the calculated HEU value is slightly closer to the LEU lifetime than it is to the HEU measurement. A large uncertainty may exist in the experimental value as several measurement methods were attempted before a noise analysis was deemed successful [5]. Like the effective delayed neutron fraction, the calculated prompt neutron lifetimes are conservative when compared to experiment. The delayed neutron fraction and prompt neutron lifetime calculations, including burnup effects, will be examined in more detail in future safety analyses prior to core conversion.

Table 4-5. Calculated prompt neutron lifetime for LEU and HEU cores.

Core configuration	**HEU core 2**	**LEU**
Non-fuel dummy element location	A2 A3 B3 B6 B9	A2 A3 B3 B6 B9
Prompt neutron lifetime (μs)	77.3	60.5
Uncertainty 1-σ (μs)	0.7	0.7

4.4 Worth of Control Mechanisms

Evaluation of control mechanism worth is an important part of model validation. MITR-II is controlled by 6 control blades and the regulating rod. Additionally, the D_2O reflector can be dumped and can be considered an auxiliary control system. As discussed below, available calibration measurements are used to benchmark calculations against experiment.

4.4.1 Control Blade Calibrations

Calibration data was available for core 2 Cd control blades 1 [35], 3 [36] and 5 [37] and for core 4 BSS control blades 2 [38] and 4 [39]. The blades were calibrated against the regulating rod or another blade for which the reactivity worth was already known according to the following procedure.

First, with the calibrated blade at a given insertion (beginning with fully inserted), the reactor was made critical using the remaining control blades and RR. Typically the known blade used was the RR at a partially withdrawn position of known worth. Next, by further inserting the blade of known worth, the reactor was again made critical with the calibration blade further withdrawn.

To build the integral worth this process is repeated until the calibrated blade has reached the full-out position. In our calculations, we have used the first critical step as a reference, and made a perturbation calculation to evaluate the worth per step. The integral worth is obtained by the sum of the worth of each step.

Figure 4-1, Figure 4-2, and Figure 4-3 present the calculated and experimental integral worth of the core 2 control blade 1, 3, and 5, respectively. Figure 4-4 and Figure 4-5 present the same for core 4 control blade 2 and 4, respectively. Use of a depleted core 4 represents a more appropriate neutron spectrum and power profile which can impact the blade worth evaluation compared to fresh fuel. The core 4 blade worth data is of particular interest since the control blades for all cores subsequent to core 4, including modern cores 178-190 and LEU, are made of borated stainless steel instead of cadmium, as used in core 1 and 2.

The archival data also considers that, for reason of symmetry, the worth of blade 6 should be the same as blade 1, the worth of the blade 2 should be the same as blade 3, and the worth of blade 4 should be the same as blade 5 [40]. These hypotheses have been tested for core 2 by using the experimental data against the non- calibrated blades. Figure 4-6, Figure 4-7, and Figure 4-8 present the calculated integral worth of the core 2 control blades 2, 4, and 6, respectively and compared them to the experimental integral worth of control blades 3, 5 and 1, respectively.

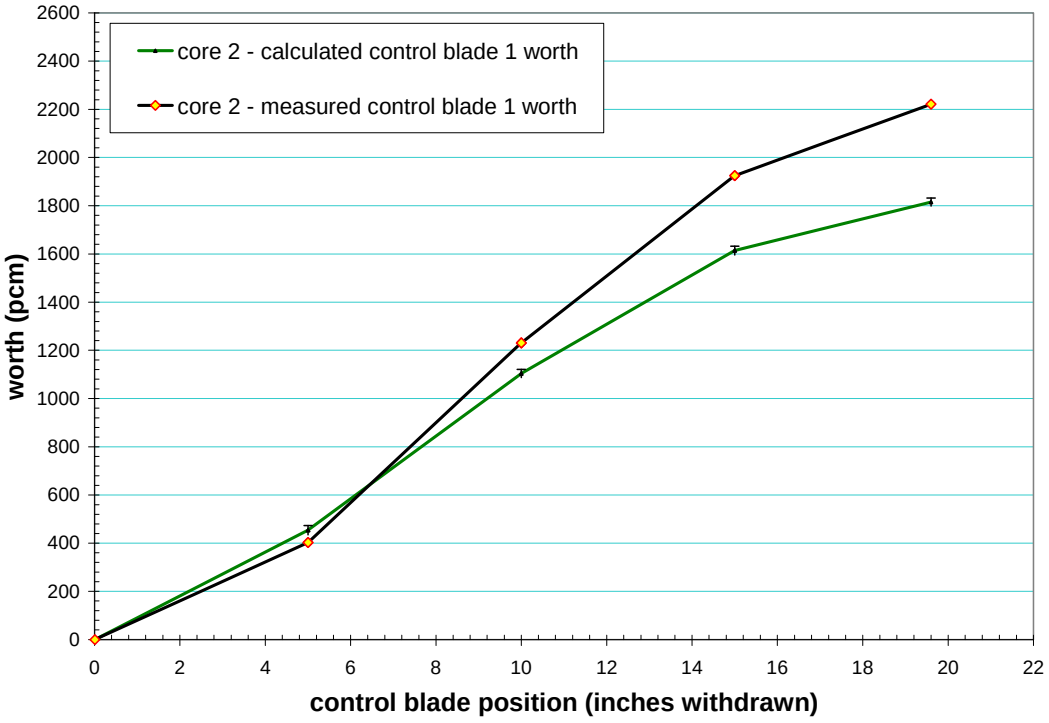

Figure 4-1. Calculated and measured worth of core 2 control blade 1.

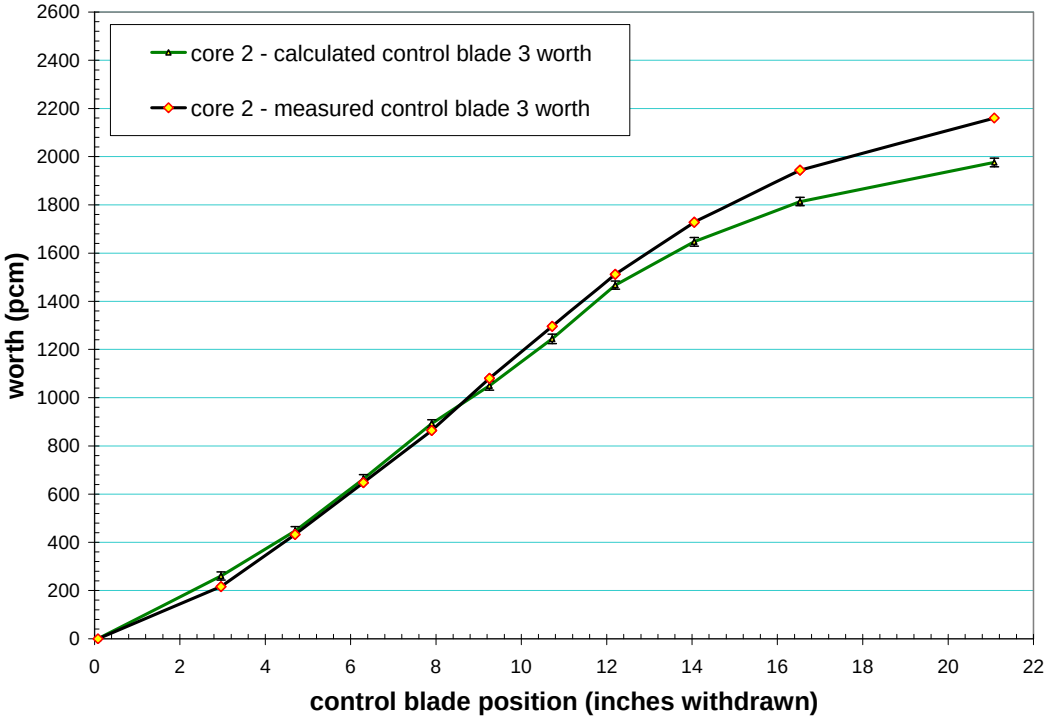

Figure 4-2. Calculated and measured worth of core 2 control blade 3.

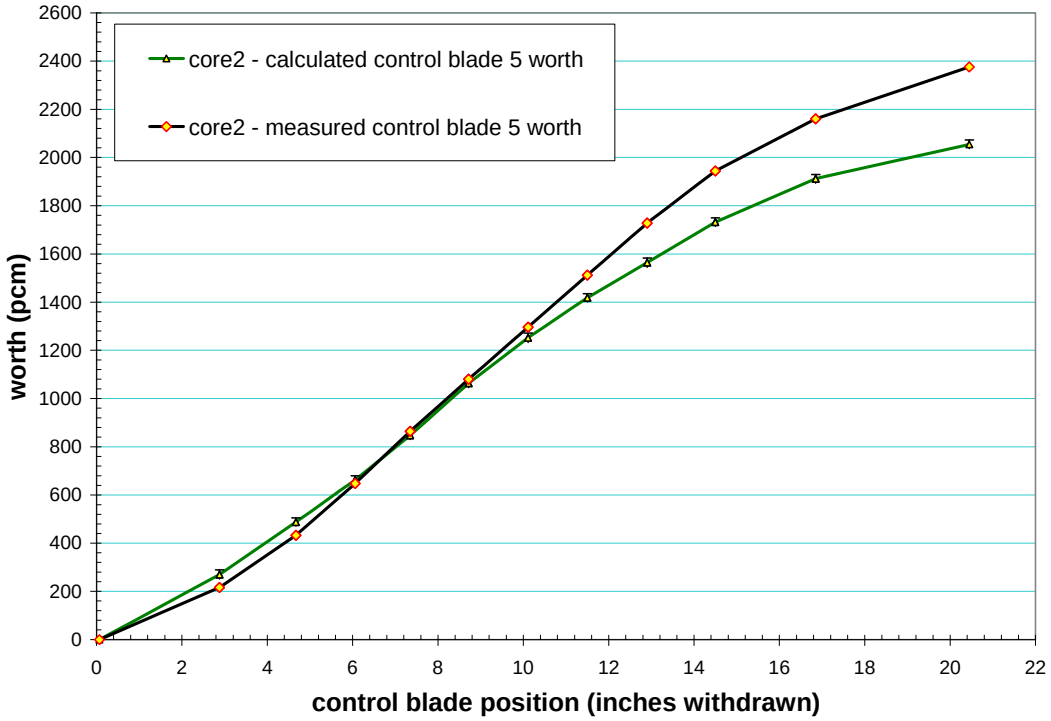

Figure 4-3. Calculated and measured worth of core 2 control blade 5.

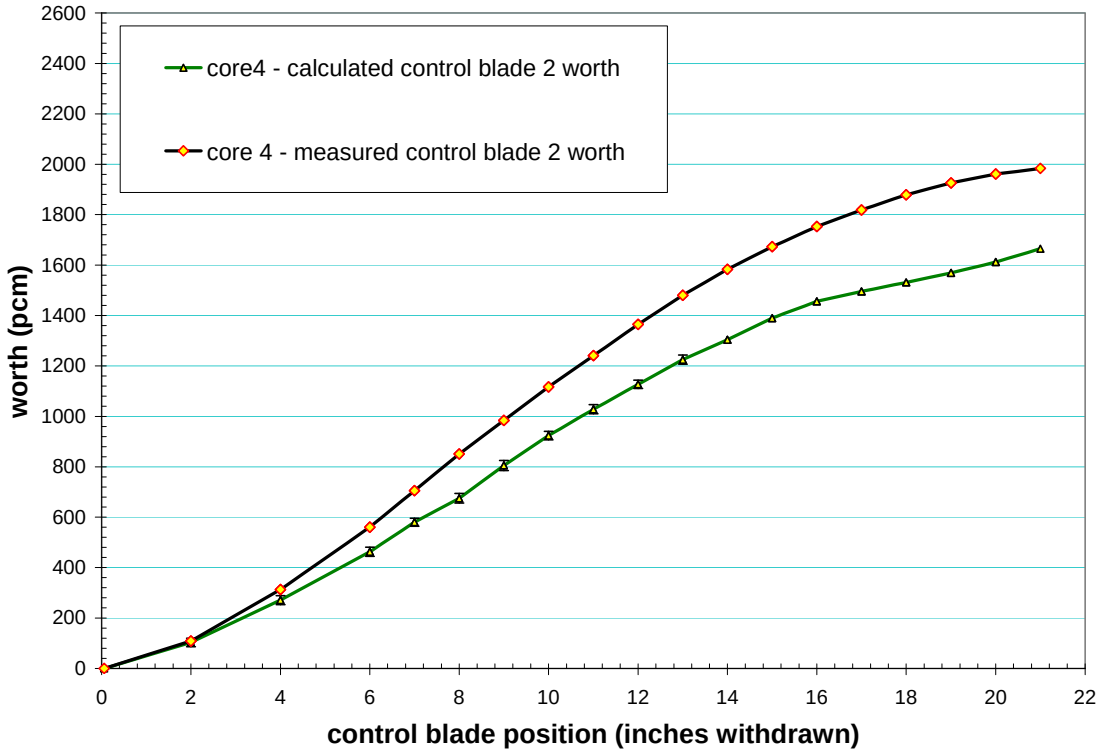

Figure 4-4. Calculated and measured worth of core 4 control blade 2.

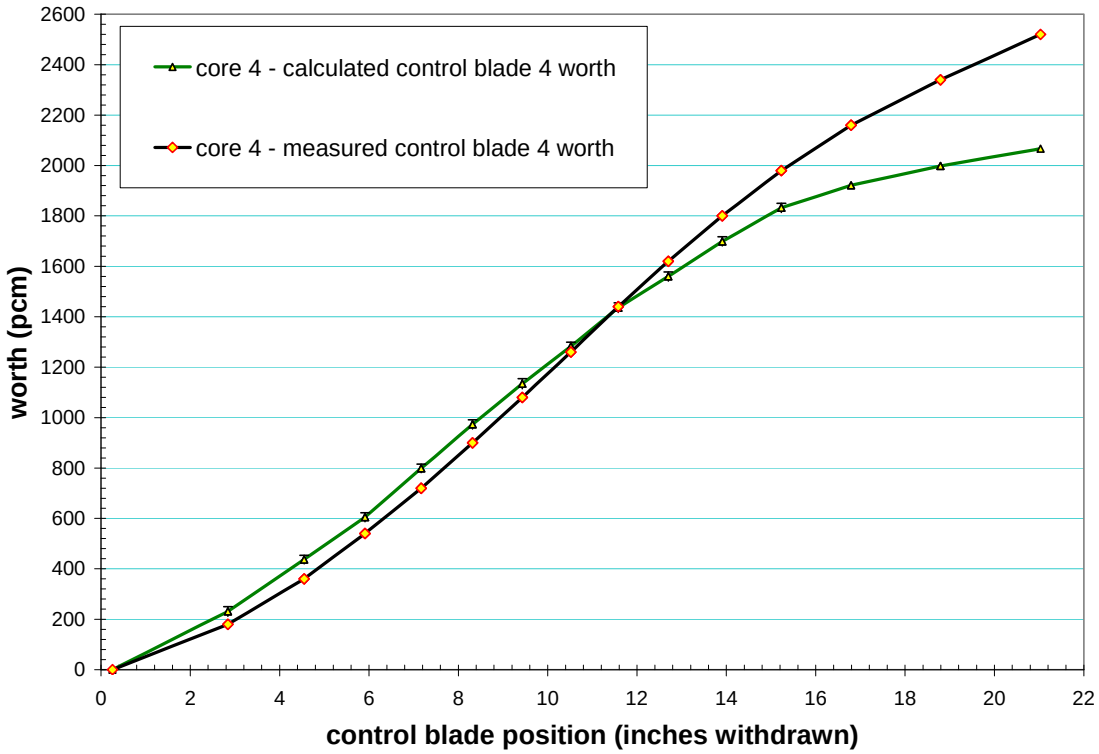

Figure 4-5. Calculated and measured worth of core 4 control blade 4.

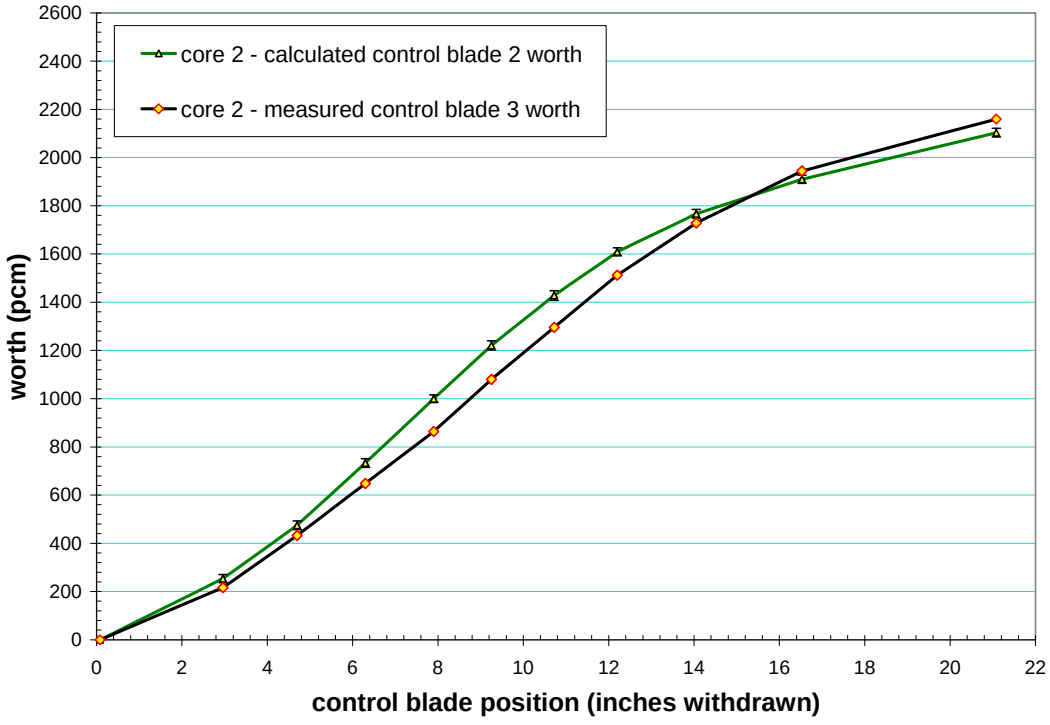

Figure 4-6. Calculated worth of core 2 control blade 2 compared to the measured worth of core 2 control blade 3 (test of symmetry hypothesis).

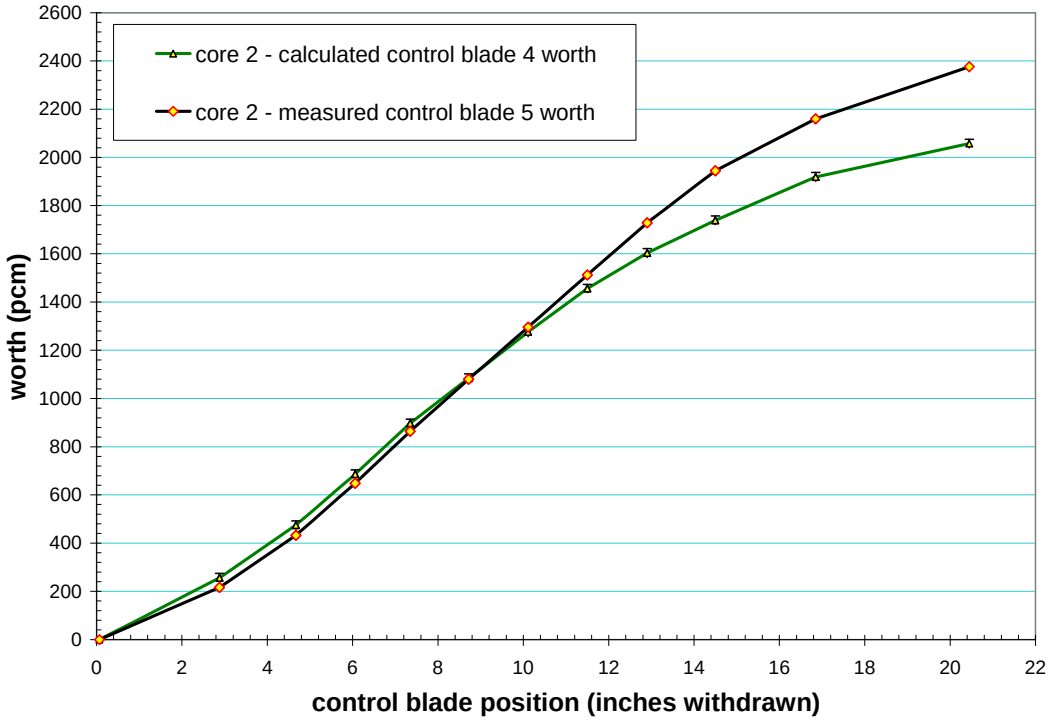

Figure 4-7. Calculated worth of core 2 control blade 4 compared to the measured worth of core 2 control blade 5 (test of symmetry hypothesis).

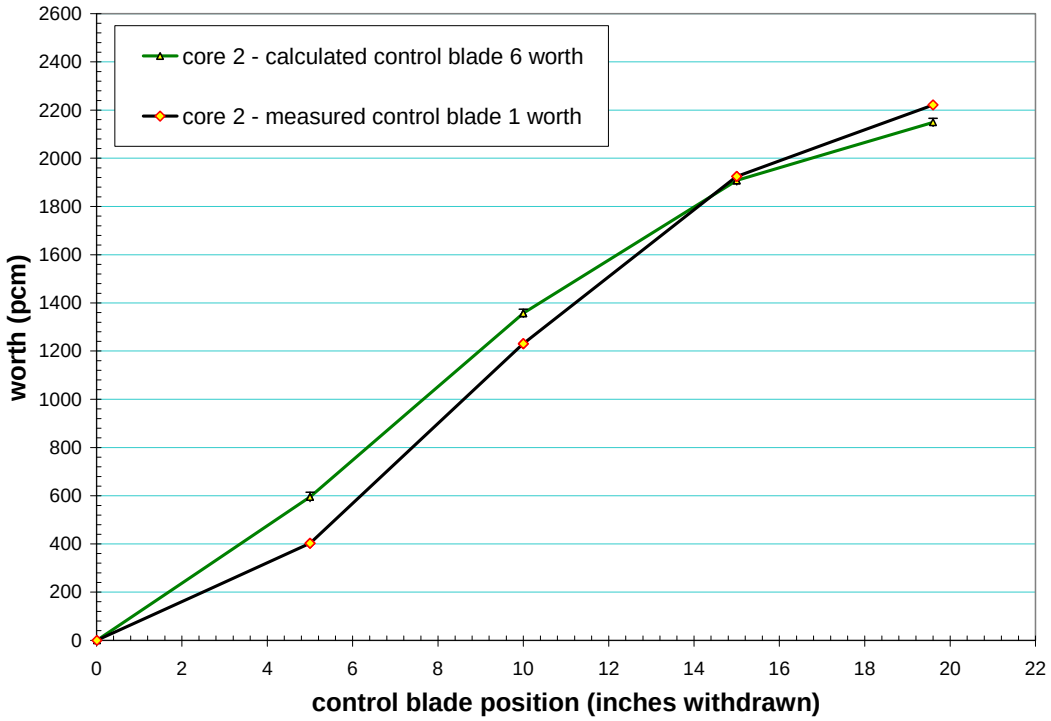

Figure 4-8. Calculated worth of core 2 control blade 6 compared to the measured worth of core 2 control blade 1 (test of symmetry hypothesis).

Each calculated integral control blade worth curve shows good agreement with experiment. Table 4-6 summarizes the calculated worth of each calibrated blade compared to experiment, and confirms control blade symmetry in these cores. The deviation from experiment is in a range of 53 to 405 pcm for core 2 and 363 to 542 pcm for core 4. Each calculated worth is lower than the experimental worth. Compared to experiment, calculations are representative of measured values and conservatively estimate the control blade worths.

Table 4-6. Summary of calculated blade worth compared to experiment.

Core 2						
Calibrated control blade	**Number of critical cases**	**RMS deviation from critical (pcm) among critical steps**	**Uncertainty 1-σ (pcm)**	**Sum of calculated worth (pcm)**	**Measured (1,3,5) or symmetrical (2,4,6) worth (pcm)**	**C-E (pcm)**
1	4	225	42	1817	2222	-405
2	10	191	47	2108	2161	-53
3	10	187	23	1982	2161	-179
4	11	189	56	2062	2377	-315
5	11	194	46	2060	2377	-317
6	4	107	79	2150	2222	-72
Core 4						
Calibrated control blade	**Number of critical cases**	**RMS deviation from critical (pcm) among critical steps**	**Uncertainty 1-σ (pcm)**	**Sum of calculated worth (pcm)**	**Measured worth (pcm)**	**C-E (pcm)**
2	18	321	50	1673	1991	-318
4	14	338	41	2074	2525	-451

Evaluation of the individual control blade worth has also been carried out for the LEU core. Since the worth of one blade is affected by the position of the other ones, each blade was evaluated by two distinct series of calculations. First the other blades are full-in, and secondly full-out. By this means, an expected range of reactivity worths is obtained. Figure 4-9, Figure 4-10, and Figure 4-11 present results obtained for blade 1, 3, and 5 respectively. As expected, shapes of blade worths for the LEU core are comparable to blade worths for the HEU core. Table 4-7 summarizes the results obtained for control blade worths of the LEU core. The worths in the LEU core are somewhat lower than that of the HEU cores since the LEU spectrum is somewhat harder and thus has a lower thermal neutron flux in the blade region.

Table 4-7. Range of reactivity worth for different blades – LEU core.

Control blade	Range of reactivity worth (pcm)	Uncertainty 1-σ (pcm)
1	1515 - 1861	< 13
3	1396 - 1856	< 13
5	1459 - 1852	< 20

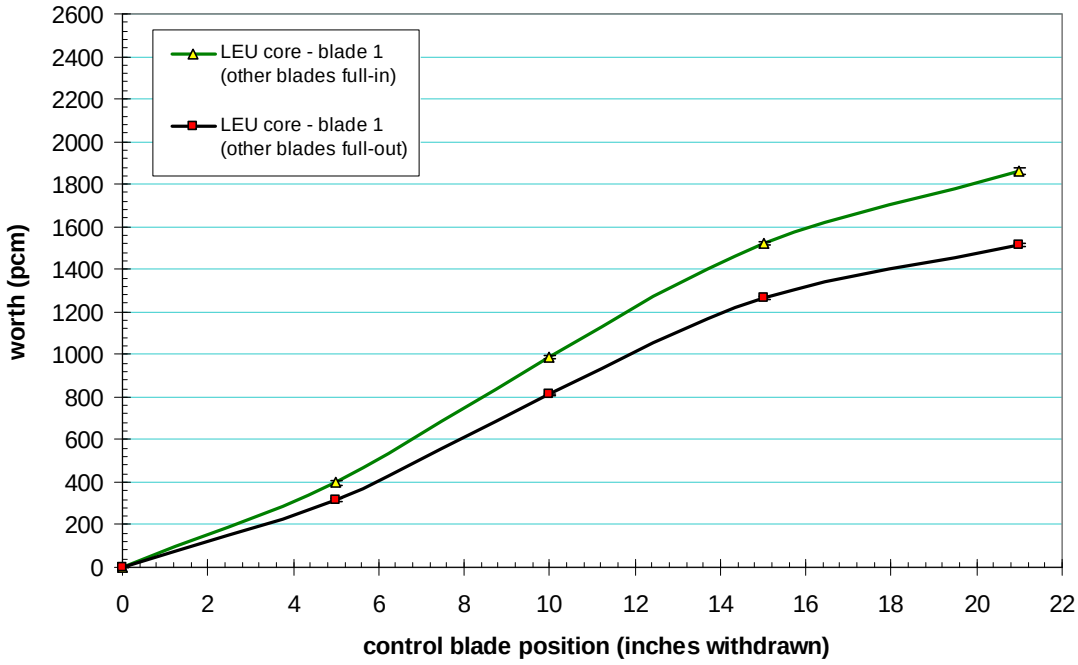

Figure 4-9. Calculated blade 1 worth for other blades full-in and full-out – LEU core.

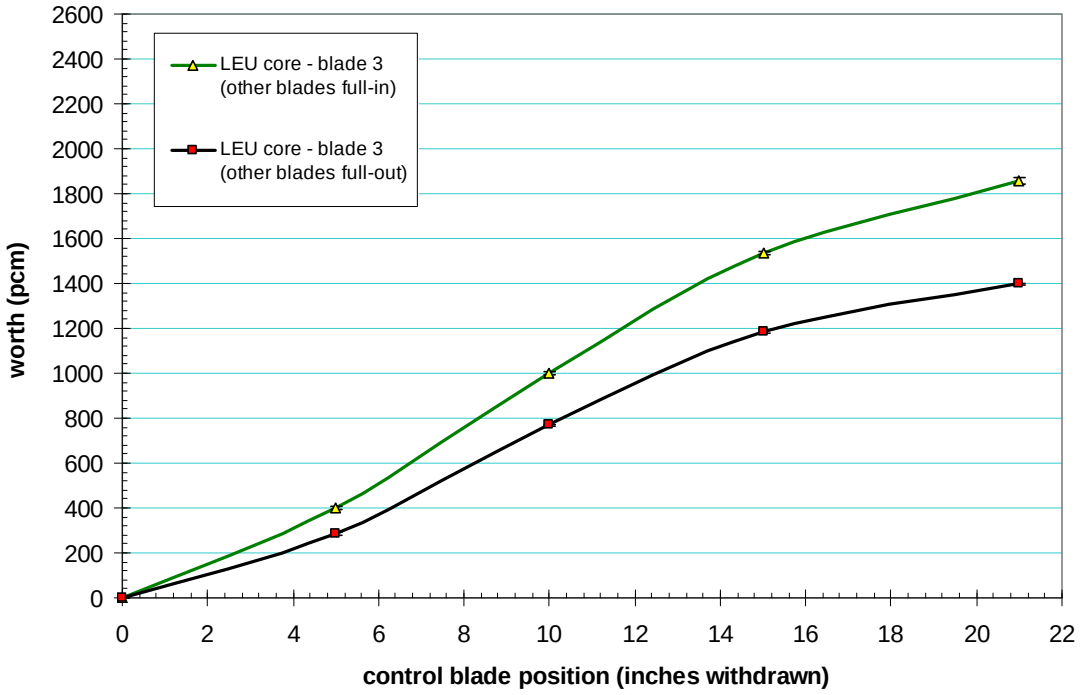

Figure 4-10. Calculated blade 3 worth for other blades full-in and full-out – LEU core.

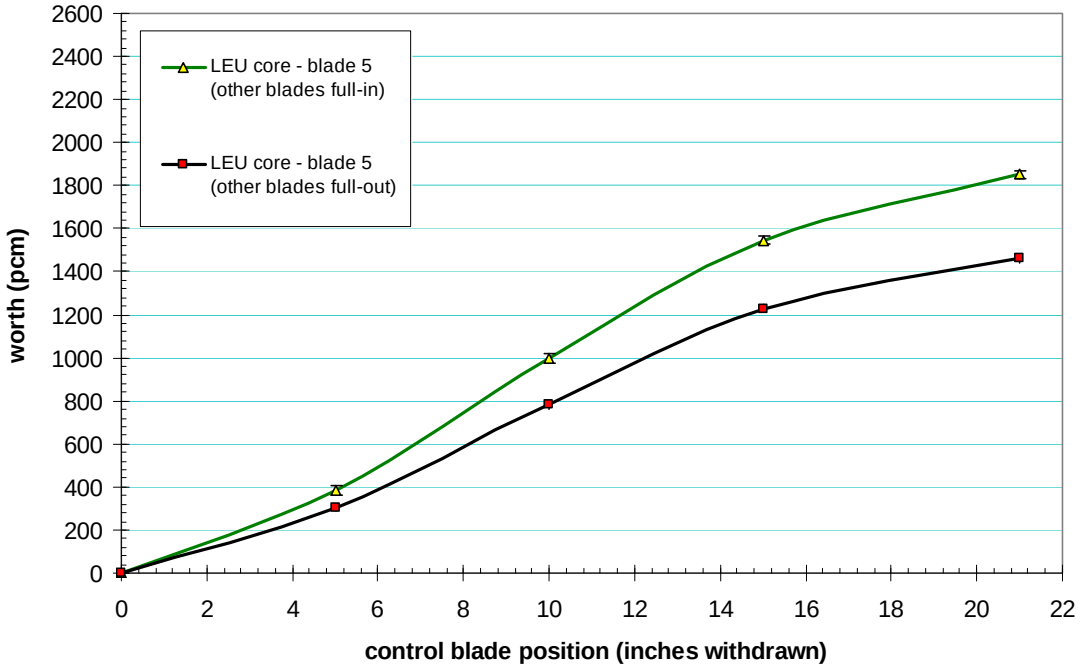

Figure 4-11. Calculated blade 5 worth for other blades full-in and full-out – LEU core.

4.4.2 Integral Shim bank worth

The MITR HEU SAR [1] refers (in Table 4-4 of that report) to a shim bank integral worth of 9927 pcm. The MIT startup report [5] refers to an integral worth in a range of 13362 – 15120 pcm. Calculated results for the different HEU and LEU cores are presented in Table 4-8. Calculations, made with the regulating rod in the full-out position, were performed by calculating Δk/k between all six blades fully inserted and fully withdrawn.

Table 4-8. Integral shim bank worth from core 1 to LEU core.

	Core 1	Core 2	Core 4	LEU
Integral shim bank worth (pcm) - regulating rod out	-11328	-12642	-11146	-10111
Uncertainty 1-σ (pcm)	41	45	14	20

4.4.3 Regulating Rod worth

Detailed experimental data regarding the calibration of the regulating rod was available. However, contrary to the control blade, the worth per critical step of this control device is small, and so the integral worths were better suited to comparing calculations to experiments among various cores. Fortunately the MIT startup report cited the integral worth of the regulating rod for different shim bank positions and for different cores [5]. Table 4-9 and Table 4-10 present results obtained by calculations compared to values given in the startup report for cores 1 and 2, respectively.

Table 4-9. Integral worth of the regulating rod for different shim bank position – core 1.

Shim bank position (inches withdrawn)	Calculated worth (pcm)	Uncertainty 1-σ (pcm)	Experimental value	Deviation from experiment (%)
7.5	130	14	134	-3.0
11	172	14	198	-13.1
16.8	214	12	269	-20.4

Table 4-10. Integral worth of the regulating rod for different shim bank position – core 2.

Shim bank position (inches withdrawn)	Calculated worth (pcm)	Uncertainty 1-σ (pcm)	Experimental value	Deviation from experiment (%)
8.5	232	18	228	1.6
11.7	282	16	322	-12.4

Calculation results are close to the experimental ones when the shim bank is close to the first critical position (7.36 and 8.2 inches for core 1 and core 2, respectively). Calculated values are lower than measured as the shim bank is more withdrawn. The phenomenon is not clearly understood but the magnitude of the discrepancy is small (≤55 pcm), and a shadowing effect between the shim bank and the regulating rod is suspected. Again, calculated values either match experiment, or are slightly conservative.

A similar calculation of regulating rod worth has been carried out for the LEU core. Figure 4-12 presents the result. The integral regulating rod worth has been evaluated from the shim bank full-in to full-out. The effect of the shim bank is clearly observed as the worth of the regulating rod doubles along the 21 inches of shim bank motion.

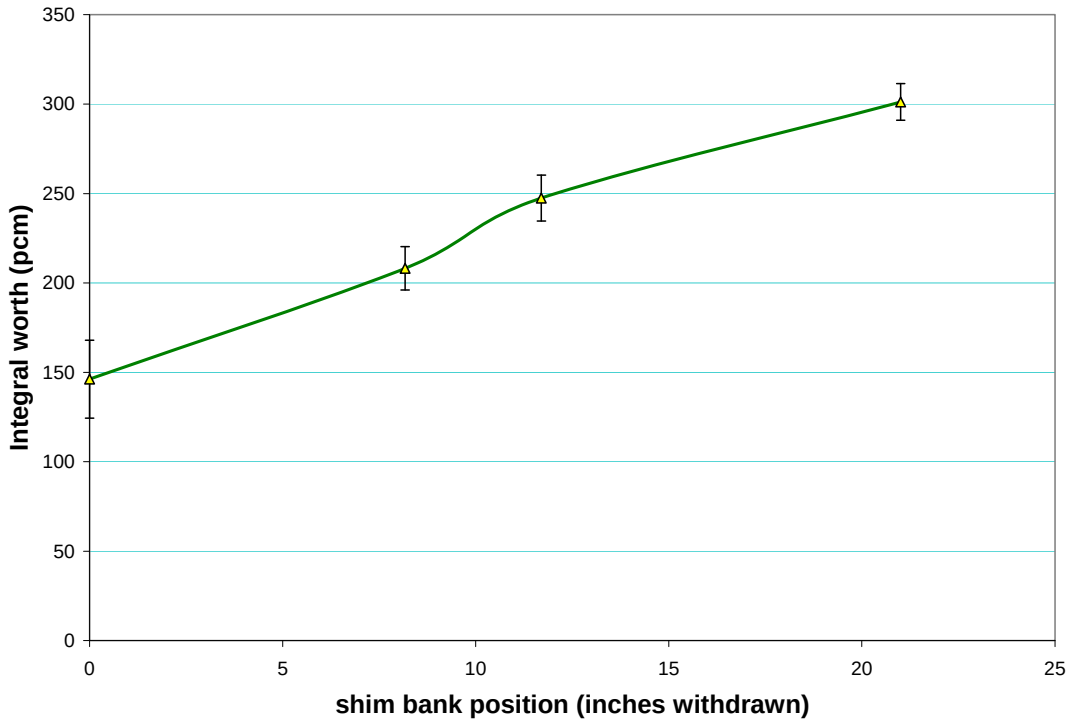

Figure 4-12. Integral regulating rod worth for different shim bank position – LEU core.

4.4.4 Shutdown Margin

In the previous section, we have shown our ability to model the shim bank and the regulating rod. Calculations give good and conservative results in comparison to the measurement. In consequence, it was credible to evaluate the shutdown margin for specific HEU and LEU cores as defined in the MITR HEU SAR [1]: the shutdown margin requirement for the MITR-II is that it be possible to shut the reactor down by at least 1% Δk/k using shim blades from the cold (10°C), xenon-free condition with both the most reactive blade and the regulating rod fully withdrawn, and with all movable samples in their most reactive state.

Shutdown margin (in terms of %Δk/k) was calculated at 10°C for the core configuration with five un-fueled dummy elements in A2 A3 B3 B6 B9, and 22 fresh, xenon-free, fuel elements. There are no movable samples present in the calculation. As calculated in Table 4-11, the most reactive blade for the LEU configuration is blade six. The shutdown margin calculated for this LEU configuration is 2.69% Δk/k (1-σ 0.01%), which exceeds the requirement. Due to LEU spectral effects, the shutdown margin is lower than that of the HEU core, but since, in the vast majority of cases there is a significant margin for HEU, a slightly lower value for LEU should not present a problem.

Table 4-11. Calculated shutdown margin for HEU and LEU cores with the same fuel loading configuration.

Shutdown margin (%) with 5 of 6 shim blades fully inserted	**HEU core 2 (1-σ 0.01%)**	**LEU (1-σ 0.01%)**
Non-fuel dummy element location	A2 A3 B3 B6 B9	A2 A3 B3 B6 B9
Control blade #1 & reg. rod out	3.35	2.73
Control blade #2 & reg. rod out	3.49	2.80
Control blade #3 & reg. rod out	3.56	2.87
Control blade #4 & reg. rod out	3.55	2.84
Control blade #5 & reg. rod out	3.50	2.84
Control blade #6 & reg. rod out	3.37	2.69

4.4.5 Heavy Water Reflector Dump

As explained previously, the D_2O reflector can be dumped, and so can be considered a secondary method of shutdown control. Experimental calibration of the reflector worth has been carried out for core 1. Detailed shim bank positions throughout the experiment were not available. However, the calibration began at a critical of 7.36 inches, and finished with subcritical counting to measure the worth. It is reasonable to presume that the shim bank was full-out during subcritical counting. In consequence, we have carried out two series of calculations. In the first, we have modeled the dumping of the reflector with the shim bank at the first critical position (7.36 inches). In the second the reflector dump was repeated with the shim bank full-out. Figure 4-13 presents the calculation results compared to experiment. As expected, calculations at a shim bank of 7.36 inches agree well with measured worth with substantial D2O present. Likewise as expected, when the D2O is substantially dumped the shim full-out calculated curve agrees well with measured worth. Importantly, the model accurately represents the reflector at both maximum insertion and full-out, and the calculated curves bound the measurements between.

The same process has been used to evaluate reflector worth for the LEU core. Figure 4-14 presents the calculation results. To make a comparison of LEU vs. HEU, the experimental data of HEU core 1 has been plotted. Results show that the total reflector dump worth for the LEU core is predicted to be reduced by 500 pcm in comparison to the HEU core 1, again consistent with spectral effects.

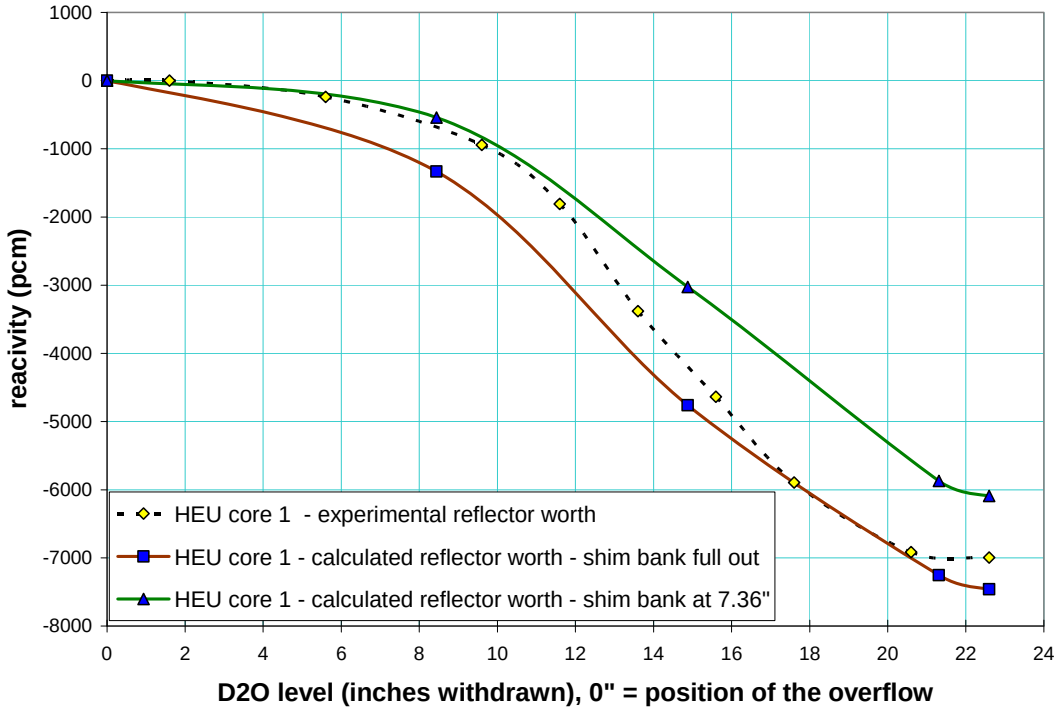

Figure 4-13. Heavy water reflector worth calculated and experimental – HEU core 1.

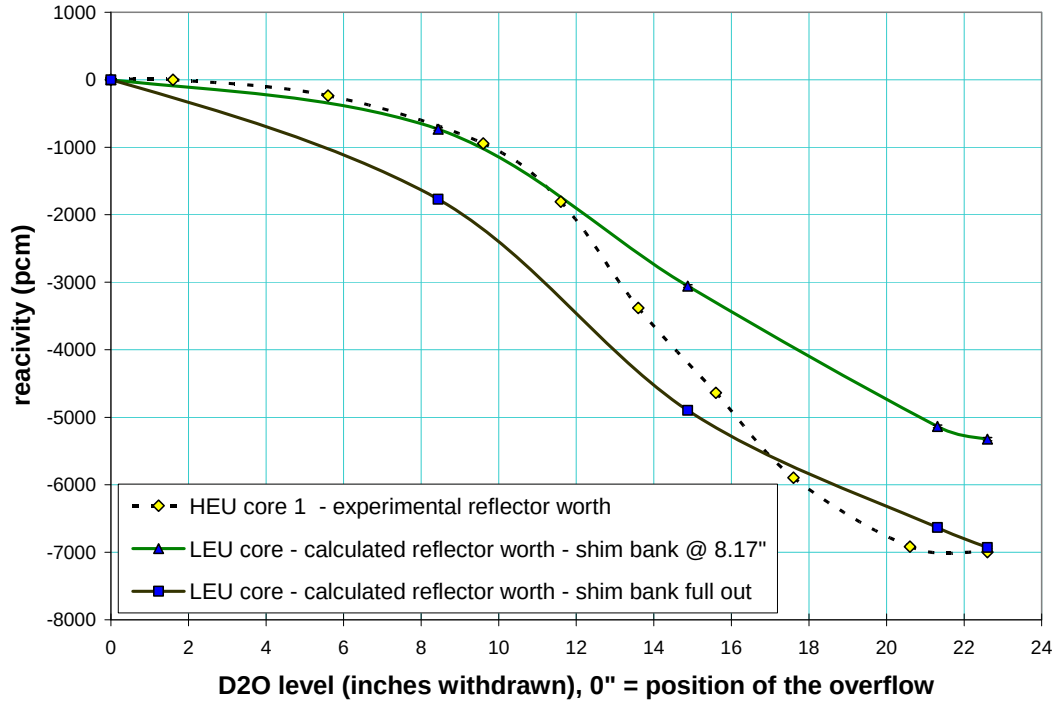

Figure 4-14. Heavy water reflector worth calculated for LEU core.

4.5 Reactivity Coefficients and Experimental Worths

4.5.1 Combined Coolant and Reflector Temperature Coefficient

The MITR-II is intentionally under-moderated so that there will be a negative coefficient of reactivity associated with the temperature of both the moderator (coolant) and the reflector. This temperature coefficient of reactivity encompasses two distinct phenomena. The first is the temperature rise of the light water because of an increase in the thermal power output of the reactor core. Any such temperature rise will insert negative reactivity by causing a hardening in the neutron spectrum. The second phenomenon is the heating of the heavy water reflector. Temperature rises of this type add negative reactivity by allowing neutron leakage to increase. This second process lags the temperature rise of the light water in the core proper.

The MITR HEU SAR cited a temperature coefficient of reactivity associated with the entire reactor (H_2O and D_2O) heat-up that varied from -4.7 to -11.8 pcm/°C over the normal band of operating temperatures from 25 to 50°C [1]. HEU and LEU calculations were performed based on changing all H_2O and D_2O in the entire reactor from 20.46°C to 76.85°C, in a single delta in order to properly account for the effect of S(α,β) cross section libraries of light and heavy water, which are available in ENDF/B-VII at these temperatures. Whereas the experimental measurements of temperature reactivity were reported in the temperature range up to 50°C [5], the range of interest extends well above this since the outlet H_2O temperature under normal LEU full-power operation of 7 MW would be in the range of 55°C.

Calculated HEU and LEU temperature coefficients are compared for identical fresh core configurations in Table 4-12. These values indicate the LEU core has a modestly lower response to temperature than the HEU core; however, the temperature coefficient remains negative and within the range given in the MITR HEU SAR [1]. Calculations also indicate these temperature coefficients are relatively stable across a variety of fuel loading patterns. Table 4-13 presents various core loadings including a depleted core 4 result of -14.3 pcm/ºC. Since neither the HEU or LEU calculations presented here account for temperature changes in the fuel, negative reactivity associated with increased fuel temperature will be studied in the future, as will burnup effects.

Table 4-12. Summary of calculated combined coolant and reflector temperature coefficients of reactivity for HEU and LEU cores.

Parameter	HEU core 2	LEU
Non-fuel dummy element location	A2 A3 B3 B6 B9	A2 A3 B3 B6 B9
Combined coolant and reflector temperature coefficient (pcm/°C)	-8.1	-6.2
Uncertainty 1-σ (pcm/°C)	0.1	0.2

Table 4-13. Comparison of calculated combined coolant and reflector temperature coefficients of reactivity among HEU cores.

Parameter	HEU core 1	HEU core 2	HEU core 4
Non-fuel dummy element location	B2 B9 ICSA in A1	A2 A3 B3 B6 B9	A1 A3 B2 B4
Combined coolant and reflector temperature coefficient (pcm/C)	-10.9	-8.1	-14.3
Uncertainty 1-sigma (pcm/C)	0.2	0.1	0.2

4.5.2 Void Coefficient

Experiments were carried out in order to estimate the void coefficient in the MITR-II core 1. Five identical aluminum plates were inserted in five coolant channels of a fuel element, and the reactivity difference measured. This experiment was made in various fuel elements which comprise the various rings of fuel in MITR-II. Two variations of this experiment have been carried out by inserting either a full aluminum plate (same length as the fuel plates) or a partial aluminum plate (6 inches in length, inserted such that bottom of perturbation plate was at the bottom of the fuel plate).

Calculations have modeled the same recorded insertion elements and channels to reproduce the inserted experimental plate drawings in the model. Results, presented in Figure 4-15 and Figure 4-16 for the full and partial aluminum plate, respectively, show good agreement with experiment. Calculated values are close to the experimental (the bias is in a range of -16 to +26%) and follow the same trend. Observed void coefficients are stronger in the A and B ring than in the C ring, which is expected since the power density is higher in the A and B ring.

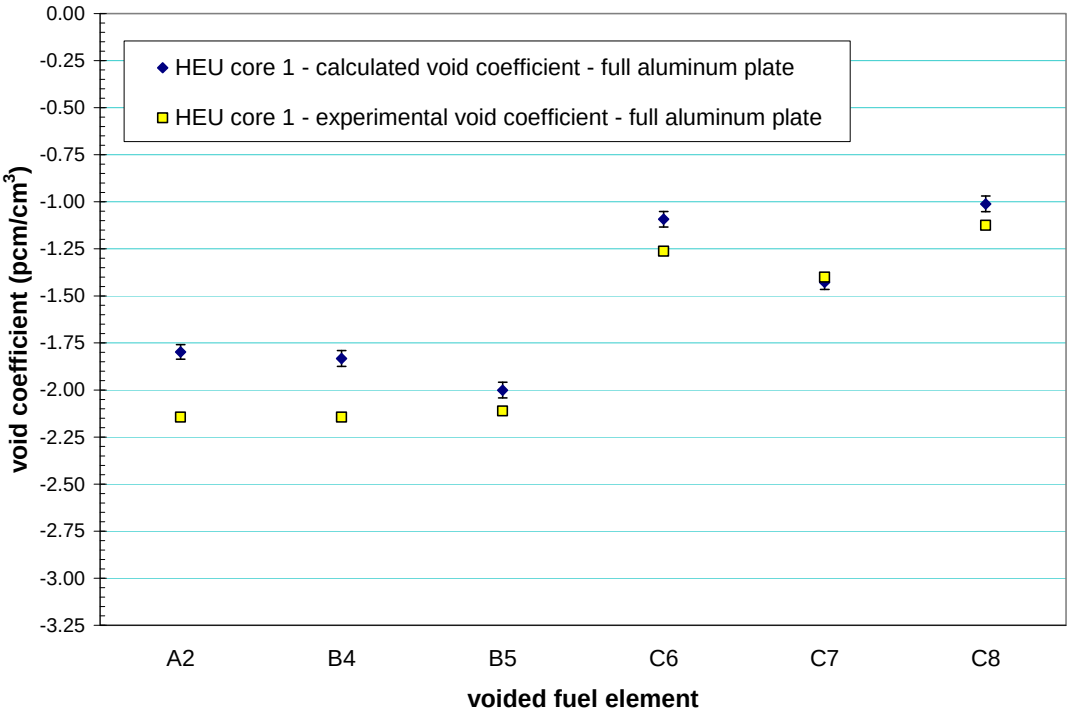

Figure 4-15. Comparison of calculated and experimental void coefficient using full aluminum plates – HEU core 1.

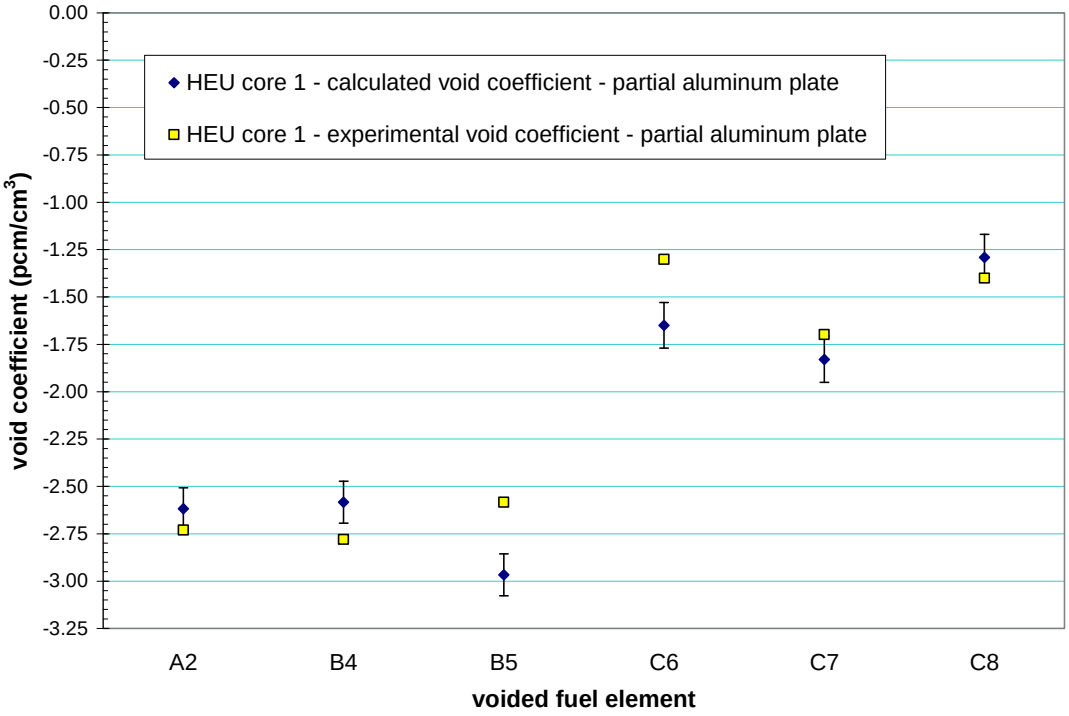

Figure 4-16. Comparison of calculated and experimental void coefficient using partial aluminum plates – HEU core 1.

The same kind of calculation has been carried out for the LEU core. However, the comparison with the HEU core is more difficult since the coolant channel volume and number differs between HEU and LEU fuel designs. In addition, the non-fueled dummy element location is also different, so it was not possible to evaluate the void coefficient in the same geometry. HEU core 1 element A2 was a non-fuel dummy element in the case of LEU core. To address these difficulties, we have chosen to present in Table 4-14 the average void coefficient per ring not on a per cm^3 of inserted (aluminum) void basis, but per percentage of void per element. Calculation uncertainty 1-σ values were always less than 1 pcm/%void per element. Calculations show that the LEU core void coefficient is reduced by 10% to 28% from the A to C-ring but is still strongly negative in all cases.

Table 4-14. Calculated Void coefficient per percentage of void per element for HEU core 1 and LEU core – Full aluminum plates were modeled.

Void coefficient	HEU core 1 calculation	LEU core calculation	Variation HEU/LEU (%)
Non-fuel dummy element location	B2 B8 ICSA in A1	A2 A3 B3 B6 B9	-
A-ring (pcm/%void per element)	-22	-20	10.2
B-ring (pcm/%void per element)	-24	-20	16.5
C-ring (pcm/%void per element)	-15	-11	28.0

4.5.3 D2O Blister Tank Worth (filled with D2O)

Table 4-5 of the MITR HEU SAR [1] gives a -55 pcm worth for draining the D_2O in the blister tank completely. Table 4-15 compares HEU and LEU calculations to this reference HEU value. HEU calculations of this tank which extends from 24 to 43 inches below the core mid-plane, shows good agreement with the experimental value. The worth of the D_2O blister tank is slightly reduced for the LEU core but is still strongly negative.

Table 4-15. Comparison of calculated and experimental D_2O blister tank worth.

D_2O blister tank worth (drained)	**HEU reference value**	**HEU Core 1**	**LEU**
Non-fuel dummy element location	-	B2 B8 ICSA in A1	A2 A3 B3 B6 B9
Worth of D_2O in blister tank (pcm)	-55.0	-53.3	-42.0
Uncertainty 1-σ (pcm)	-	5.7	5.0
Deviation from reference value (%)	-	-3%	-24%

4.5.4 Fuel Element Worth

MIT staff carried out experiments in order to evaluate the worth of fuel elements in MITR-II core 1. The calibrated element was replaced by a specially constructed element, known by designation 'element 001', where the plates were filled only by aluminum instead of fuel meat. The measured difference of reactivity gives the worth of the element. HEU core calculations presented in Figure 4-17 show good agreement with experiment. Calculation uncertainties are not presented on the figure but are always below 20 pcm at 1-σ. Compared to the other rings, the bias is larger in the A-ring (-19%) but still reasonable. LEU calculations are also plotted in the figure. Results show that the LEU fuel element worth trends similarly by ring, and that the overall magnitude is similar but reduced by 200-400 pcm depending on the element location.

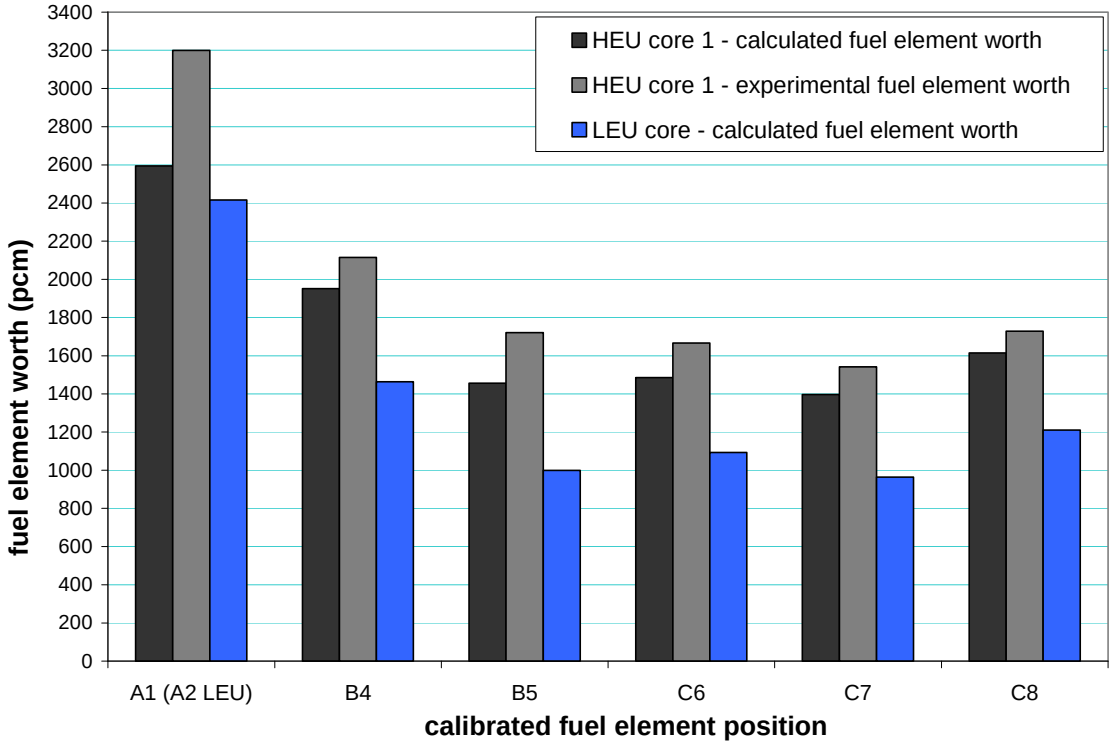

Figure 4-17. Experimental and calculated fuel element worth.

4.5.5 Dummy Element Worth

Specific experimental data on the non-fuel dummy element worth was not available; however, the MITR startup report [5] specifies an average value of 600 pcm for a dummy element present in the B-ring of core 2. Calculations of individual dummy elements were carried out replacing the calibrated element by light water. Results, presented in Table 4-16, show good agreement with experimental data except for the B9 location. This discrepancy can be explained by the fact that the B9 dummy has 4 sides adjacent to fuel elements, whereas the other dummies have only 3 sides adjacent to fuel elements. A calculation has been carried out switching the location of the fuel element in the A-ring with another A-ring dummy. In this manner, the number of fuel elements neighboring location B9 was artificially modified to be 3 by switching the A1 fuel and A3 dummy elements so that A3 is fueled and A1 a dummy. It is possible that the recorded experiment records may be lacking detail on the element arrangement in this case, since re-evaluation of the worth in this manner has given a result closely matching 600 pcm, as shown in Table 4-16.

Dummy element worth has also been evaluated for the LEU core. Results are presented in Table 4-17. In comparison to the HEU core, the LEU core dummy worth increases significantly by more than 400 pcm. The same increased worth observed for the dummy located in the B9 location is observed for LEU. As for the HEU core, this difference disappears when a switch is made in the A-ring element.

Table 4-16. Calculated and experimental worth of the non-fuel dummy element – HEU core 2.

Non-fuel dummy element location	Worth MCNP (pcm)	Uncertainty 1-σ (pcm)	Experimental worth (pcm)	Deviation from experiment
B3	-590	13	-600	1.7%
B6	-531	15	-600	11.5%
B9 (A1 fuel)	-1144	12	unclear	n/a
B9 (if A1 dummy)	-598	14	-600	0.4%

Table 4-17. Calculated worth of the non-fuel dummy element – LEU core.

Non-fuel dummy element location	Worth MCNP (pcm)	Uncertainty 1-σ (pcm)
B3	-958	13
B6	-939	12
B9 (A1 fuel)	-1512	14
B9 (if A1 dummy)	-972	13

5 Comparison of Model Results to Recent Experimental Benchmark Data

5.1 Overview of Recent Experimental Benchmark Data

In addition to comparing MCNP model results to experimental benchmarks from the historical start-up period of the MITR-II reactor 1975-1976, calculations have been performed on more recent cores from the period 2007-2009. Whereas the former set of cores (cores 1 to 4) were fresh, or very nearly fresh, the sequence of cores 178 to 190 represents periodic refueling.

5.1.1 Modern HEU benchmark cores

A model specific to the modern MIT reactor internal structure, control devices, and fuel composition was used for calculations of these modern cores 178 – 190. Physical modifications between the cores are detailed in Table 4-1.

The methodology for analysis of depleted cores requires burnup chain analysis such as is found in ORIGEN [41] or REBUS [42] depletion codes. A wide set of comparisons has been reported previously for the MITR-II reactor for various codes using both transport and diffusion theory calculations, for example in references [3], [43] and [44]. These comparisons contained fuel shuffling and modeling of modern core sequences similar to that described in this report, and produced some reasonable agreement in code to code comparisons.

However, beyond comparison of one code to another, it is highly desirable for verification and validation purposes to complete a comparison of model calculations against available experimental benchmark data. Whereas previous comparisons to historical start-up reference data for undepleted cores had been performed, agreement between modeled and experimental conditions was limited, as discussed in section 4.1 of this report. In addition, comparison of a modern depleted core to experimental measurements has been performed with the objective to establish a basis for safety calculations for the conversion from HEU to LEU fuel.

The model presented in Chapter 2 of this report establishes a high-fidelity core representation of the MITR-II reactor which encompasses both modern as well as the start-up cores discussed previously.

5.1.2 Depleted Core Methodology

Since the last fresh core operated at MITR-II in 1975, a direct depletion of elements from 1975 to present is not practicable. Instead, initial values of burnup for each of the elements was obtained using the diffusion theory code CITATION [45] which has been used to calculate values used for ongoing safety analyses prior to each refueling.

Before implementing the fuel shuffling presented in section 5.2, depleted fuel elements were generated to represent the element-average fuel burnup values taken from CITATION calculations. This was performed by burning an all fresh modern core over a period sufficient to deplete the elements across the range given by CITATION.

The MCNP model subdivided each element into six axial nodes in each of the 24 fuel elements present. Thus 144 material zones were depleted throughout the reactor, where each of the 15 plates in each of the six axial segments shared the same material composition. Without shuffling, depleted fuel and fission product densities were obtained in each of the six element axial segments using MCNP5 [46] in an **MC**NP - **O**RIGEN coupled **De**pletion calculation software package known as MCODE [47]. Besides the element average ^{235}U mass taken directly from CITATION, all fission products and transmuted fuel compositions, including axial shape within the elements six segments, were calculated directly from MCODE. Due to the flexibility for MITR fuel elements to be flipped axially as well as rotated in the horizontal plane, the depletion was performed without control blades inserted to best represent the axial burnup profile of an average element. Each element average ^{235}U mass was matched at the specific depletion step required, and in the same core fuel location specified for first loading into the shuffling pattern. After these values were obtained, short-lived fission products were decayed appropriately before implementing the element into the shuffling scheme. Due to the lack of shuffling, and the absence of control rods in the depletion, the first core fueled with these elements will only approximate the actual fuel compositions.

5.2 Core 178 – 190 Experimental Benchmark Data

5.2.1 Refueling Operations for 13 Cores

Due to the approximate representation of the initial burnup step discussed in 5.1.2, a sequence of core refueling was selected to continue the fuel depletion in a more realistic manner. Thirteen actual cores were represented based on the recorded operations of fuel movements, cycle length, and approximate power. These thirteen cores are MITR-II cores 178 to 190, and Table 5-1 presents the fuel loading history over the course of two years. The operational history was modeled beginning with the end of cycle 178, and all fuel operations were respected including flipping of fuel.

5.2.2 Experimental Measurements for 13 Cores

Experimental measurements representing the fuel operating cycle of the reactor are presented in Table 5-2, where measured values for the control blade shim bank position are recorded at beginning and end of cycle. The end of cycle measured values were taken at xenon equilibrium conditions where possible. Additionally, approximate average power over the course of the cycle, and at end of cycle are tabulated. The presence of non-fuel sample assembly elements is also included along with their location in the reactor core. These non-fuel elements are inserted in place of the standard solid (with cooling hole) aluminum dummy elements, and modeled for accuracy of the criticality calculations.

Table 5-1. MITR-II fuel loading pattern for Cores 178 to 190.

Core	178	179	180	181	182	183	184	185	186	187	188	189	190
Location	5/4/07	7/17/07	10/13/07	1/5/08	3/8/08	5/23/08	6/4/08	7/25/08	9/23/08	12/17/08	2/7/09	3/13/09	5/28/09
A1	Non-fuel solid dummy element with cooling hole												
A2	MIT-323					MIT-339f						MIT-345	
A3	Non-fuel solid dummy element with cooling hole												
B1	MIT-335				MIT-344 new							MIT-354 new	
B2	MIT-338					MIT-331				MIT-351 new			
B3	Non-fuel solid dummy element with cooling hole												
B4	MIT-336	MIT-341 new						MIT-347 new				MIT-355 new	
B5	MIT-339				MIT-345 new					MIT-352 new			
B6	MIT-331	MIT-342 new						MIT-348 new					
B7	MIT-337				MIT-346 new							MIT-356 new	
B8	MIT-340					MIT-336f				MIT-353 new			
B9	MIT-334	MIT-343 new						MIT-349 new					
C1	MIT-302			MIT-325(C14)f							MIT-299(C15)		
C2	MIT-303		MIT-288(C2)		MIT-282f				MIT-326f				
C3	MIT-300		MIT-319(A2)					MIT-301f			MIT-290(C8)		
C4	MIT-305			MIT-332(B2)	MIT-303f				MIT-340f				
C5	MIT-282	MIT-281(C2)			MIT-304(C6)f				MIT307(C14)				MIT-341f
C6	MIT-279			MIT-330(B4)	MIT-295(C11)			MIT-306f				MIT-297(C7)	MIT-342f
C7	MIT-324			MIT-305			MIT-334f						
C8	MIT-306							MIT-295f			MIT-323		
C9	MIT-318		MIT-326(B5)		MIT-288f		MIT-324f						
C10	MIT-322		MIT-292(C1)f						MIT-294(C10)			MIT-330f	
C11	MIT-301					MIT-333(B6)f							
C12	MIT-285			MIT-300			MIT-293(C9)f			MIT-332f			
C13	MIT-327									MIT-317(A2)	MIT-317f		
C14	MIT-328									MIT-338f			
C15	MIT-329					MIT-337						MIT-335	
# of fuel moves	22 to begin model	4	4	5	8	5	3	6	4	6	4	7	2

Notes: "f" indicated element is flipped before insertion
"new" indicates 508 g 235U element
"( )" indicates core location element occupied prior to storage

Table 5-2. MITR-II Operational History for Cores 178 to 190.

Core number	179	180	181	182	183	184	185	186	187	188	189	190
Core operation (MWHr)	5824	4242	5789	6873	838	3602	3993	5970	4010	2664	6567	5475
Startup shim bank (inches withdrawn)	8.32	9.27	9.86	10.15	10.86	9.98	9.6	9.95	9.31	9.99	8.3	9.45
Reg. rod (inches withdrawn)	3.25	3.65	3.89	3.1	1.3	0.5	8.97	2	2.5	2.4	2.09	1.82
Approx. average power (MW)	4.5	4.8	4.6	4.6	4.65	4.0	4.0	4.7	4.9	4.6	4.6	4
Shim bank at shutdown (inches withdrawn)	15.34	16.07	17.06	19.75	15.5	16.3	16.5	18.12	16.3	16.3	14.68	15.15
Power just before shutdown (MW)	-	4.7	4.7	4.4	-	4.0	4.3	-	4.9	4.6	4.15	2.6
Sample assembly location	ACI (B3)	-	-	-	-	-	-	-	-	-	ACI (B3)	ACI (B3)
Equivalent days in cycle	54	37	52	62	8	38	42	53	34	24	59	57

5.2.3 Core 178 – 190 Model Depletion Calculations

The MITR-II model specific to the geometry and materials representing cores 178-190, as described in Chapter 2, was used during core depletion calculations using the methodology described in section 5.1.2.

The series of fuel reloadings and core operating cycles were used to deplete cores 179 through 190 using MCODE. Each core is modeled at the average power at the critical control blade position using a criticality search. Appropriate time steps have been chosen to calculate depletion during the first days as xenon reaches equilibrium.

At reloadings, additional new fuel elements are typically added three at a time, and ordinarily into the B-ring in order to provide sufficient excess reactivity and also limit peaking factors by avoiding fresh A-ring fuel. Depleted fuel that reaches sufficiently high burnup is discharged, and other elements are moved in and out of storage as needed to represent the historical refueling. The shutdown time between cores has been assumed to be a representative 5 days, and this time is used to take into account the proper decay of fission products with ORIGEN. As elements are brought into the core from storage, these have been depleted according to the method described in 5.1.2, and their fission products have been allowed to decay during the 5 day shutdowns between cores. At the point of core 190, all elements initially present in the reactor for core 178 no longer remain in the core. For benchmarks against experimental data, the representation of burnup is less accurate for the earliest cores, and improves after a more realistic axial burnup profile has been allowed to develop.

It should be noted that due to the large number of fueling operations and elements in-core, fresh, and retrieved from storage, MITR continues to load stored fuel in this sequence even at core 189. The bundles retrieved from storage continue to have some impact as they developed the physical burnup profile during the 13 core depletion. In order to completely eliminate this effect and determine whether reactor calculations would be impacted would be difficult presently, as a larger number of modeling sequences would need to be defined in addition to the more than 80 shuffling operations on 62 elements. This refueling includes 59 fuel elements representing, initially, 30 kg of ^{235}U.

5.3 Model results of Cores 178 – 190

5.3.1 Methods for Calculation Comparison to Experiment

At the conclusion of depleting the 13 cores, a variety of information is available for comparison to experimental measurement. Initially, comparison of estimated critical positions from the critical search at each point in the core sequence can be made for which data is available. If the critical search is set to find the shim bank height which has a k-effective distinct from 1.0, then an impact due to the model bias could be included. The model bias has been characterized in Chapter 4 of this report, and has been observed

to be relatively constant over a wide range of critical control blade positions and core configurations.

However, instead of selecting a value for a critical search which would include a model bias based on these calculations, and which could arguably be set over a range of values, the critical search was set to deplete for a modeled k-effective of 1.0. Reactivity was used as a comparison to experimental critical positions by calculating k-effective separately from the depletion once the beginning of cycle (BOC) and end of cycle (EOC) depleted material densities have been obtained. This methodology has the advantage that a relative measure such as a control blade position deviation is not used since these are specific to core configuration, burnup state (BOC, EOC), and vary widely among various reactors. Reactivity as an absolute quantification of deviation from the experiment can be understood in relation to the reactivity discrepancies typically modeled across a range of different reactors other than MITR-II.

5.3.2 Calculated Reactivity of Modeled Cores 178 – 190

Figure 5-1 presents results of the modeled reactivity at BOC and EOC for the twelve reloadings of cores 179-190. In these calculations the BOC shim bank height and regulating rod position were as specified in the data given in section 5.2.2. EOC shim bank height was also modeled with the data in section 5.2.2. No EOC regulating rod position was known, and so the EOC regulating rod was placed at the average of the available data presented in 5.2.2 to represent the wide variation while operating this fine control mechanism. Due to the small temperature range, and so as not to introduce issues with S(α,β) cross section library temperatures, there was no change in the definition of water between the depletion conditions and the reactivity calculation which was left in the operational conditions discussed in section 3.3. Depletion calculation uncertainties, where critical search at each time step of the 12 cores required multiple calculations, were performed with a k-effective 1-σ of approximately 70 pcm. When calculating k-effective at the measured critical height, there was an uncertainty 1-$\sigma \leq$ 13 pcm.

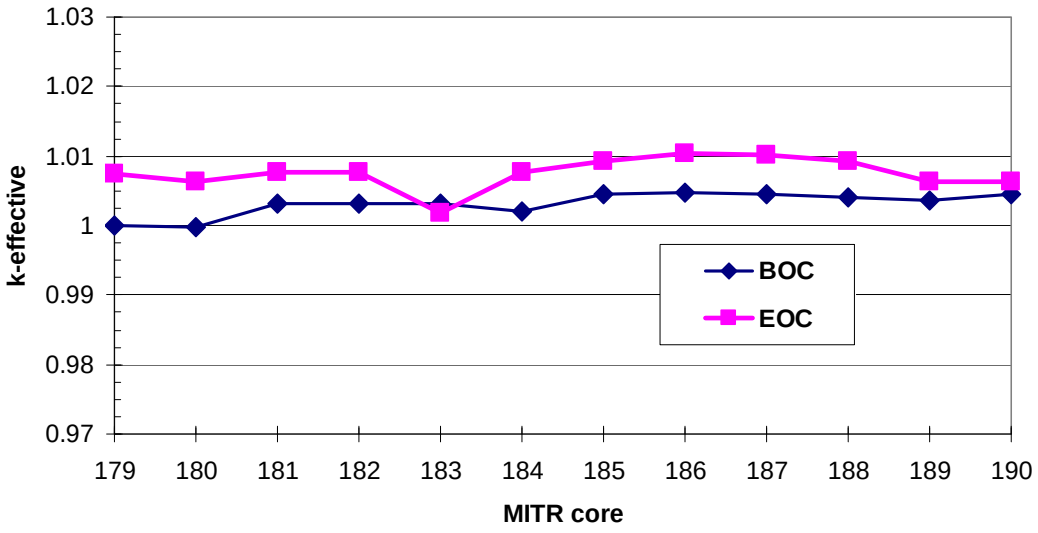

Figure 5-1. Reactivity for BOC and EOC representing two years of historical operation during cores 179-90.

Table 5-3. Reactivity results of the depletion of twelve historical core fuel loadings 179 - 190.

CORE	BOC k-effective	EOC k-effective	BOC excess reactivity	EOC excess reactivity
179	0.99995	1.00753	0.0%	0.7%
180	0.99977	1.00626	0.0%	0.6%
181	1.00317	1.00762	0.3%	0.8%
182	1.00314	1.00778	0.3%	0.8%
183	1.00318	1.00176	0.3%	0.2%
184	1.00214	1.00760	0.2%	0.8%
185	1.00451	1.00918	0.4%	0.9%
186	1.00465	1.01031	0.5%	1.0%
187	1.00453	1.01025	0.5%	1.0%
188	1.00403	1.00928	0.4%	0.9%
189	1.00353	1.00626	0.4%	0.6%
190	1.00451	1.00626	0.4%	0.6%
		Average	**0.3%**	**0.7%**
		1-σ	**0.2%**	**0.2%**

The reactivity is steady throughout the course of the depletion, as shown in Table 5-3, where an average BOC reactivity bias of 0.31% remains steady throughout the course of the 12 depletions, with a 0.2% 1-sigma standard deviation in excess reactivity. The only points which are below k-effective of one are cores 178 and 179 BOC where as discussed in section 5.2.3, the core has had the least time to develop a representative axial burnup profile. EOC bias is higher, at 0.75%, but shows a similarly tight trend as BOC with a 1-sigma standard deviation of 0.2%. Note that core 183 EOC reactivity is an experimental data point with high uncertainty. Core 183 EOC is the only core where the EOC shim bank (15.5 inches withdrawn) is further inserted than near xenon equilibrium (16.85 inches withdrawn). Core 183 only operated for a small fraction of the typical time (838 MWHr).

Overall, good agreement is seen with the bias found in Chapter 4 of this report, where the reactivity bias of the representative historical cores without fixed Cd absorbers was shown to be typically in the range of +0.2 to +0.3%Δk/k. The EOC bias is consistently higher than BOC; however, after each refueling, the BOC bias returns to a consistent level. If inaccuracies in the depletion were causing the increased EOC bias, then we would expect a growing bias over the course of these 13 cores. Currently there are no divisions other than axial for depletion zones in the element. All 15 plates in each of the six axial divisions share the same material density. Since the bias decreases at each BOC, short-lived fission products may be studied with a finer depletion spatial discretization to determine if improved short-lived fission product worth impacts the EOC to BOC delta.

6 Conclusions

This report documents the calculational results of the MITR HEU and LEU models compared to existing experimental HEU data.

The analyses presented in this report show that the MITR reactor can be operated safely with the new LEU fuel element if the UMo fuel can be qualified and manufactured. Nevertheless, as has always been true for reactor conversion projects, full safety analyses need to be performed and regulatory approvals received before the reactor will be able to convert.

It is important to note that the UMo monolithic fuel is not yet qualified or commercially available. The partnership of the GTRI Reactor Conversion Program with MITR and the DOE qualification program is a key step toward qualifying the monolithic UMo fuel and toward clarifying the specifications that will be supported for this new fuel. The positive results reported at this time are predicated on the best information available to date for fuel performance and feasibility. The technical analyses that we have completed indicate that the use of the LEU fuel element design allows MITR to operate with neutronic characteristics within prior bounds. Detailed studies of an LEU core operating with partial refueling remain to be studied in future work.

Finally, we must also note that the economic feasibility of conversion cannot be established until commercial availability of the fuel has been developed, including credible fuel cost projections. MITR and GTRI must maintain close contact in order to pursue analyses and potential redesigns once key factors are better understood.

7 Acknowledgements

This report was produced by MITR and Argonne staff working in close collaboration. In particular, the authors express their gratitude to Benoit Dionne, Justin Thomas, Arnold Olson, John Stillman, Ben Forget, Edward E. Pilat, and Paul Romano for sharing their expertise and efforts.

8 References

[1] MITR Staff, "Safety Analysis Report for the MIT Research Reactor (MITR-II)," MIT Nuclear Reactor Laboratory, October 2010.

[2] MITR-II "Fuel Element Assembly," drawing R3F-201-4, MIT Nuclear Reactor Laboratory, Massachusetts Institute of Technology, Cambridge, Massachusetts.

[3] T. Newton, L-W Hu, G.E. Kohse, E.E. Pilat, B. Forget, P.K. Romano, Y-C Ko, S. Wong, Y. Wang, B. Dionne, J. Thomas and A. Olson, , "Completion of Feasibility Studies on Using LEU Fuel in the MIT Reactor," Proceedings of the RERTR Conference, Beijing, China, Nov. 2009.

[4] E G & G Idaho, "Specification for Massachusetts Institute of Technology Fuel Elements," Specification TRTR-3, Idaho Falls, ID, rev. 1.

[5] "MITR-II Start-up Report," MITNE-198, Nuclear Engineering Dept., Massachusetts Institute of Technology, Cambridge, Massachusetts, January 1977.

[6] F.B. Haghighi, M.S. Thesis, "Natural Convection Analysis of the MITR-II During Loss of Flow Accidents," Massachusetts Institute of Technology, Cambridge, Massachusetts, August 1977.

[7] T.H. Newton, Jr., Dissertation "Development of a Low Enrichment Uranium Core for the MIT Reactor," Massachusetts Institute of Technology, Cambridge, Massachusetts, 2006.

[8] IAEA-TECDOC-683, "Research Reactor Core Conversion Guidebook Vol. 4 Appendix I, IAEA, Vienna, Austria, 1992.

[9] Private communication with Benoit Dionne of Argonne National, RERTR, November 17, 2009.

[10] A.B. Robinson, G.S. Chang, D.D. Keiser, Jr., D.M. Wachs, and D.L. Porter, "Irradiation Performance of U-Mo Alloy Based 'Monolithic' Plate-Type Fuel – Design Selection," Idaho National Laboratory document INL/EXT-09-16807 Rev. 0, August 2009.

[11] J. Rest, Y.S. Kim, G.L. Hofman, M.K. Meyer and S.L. Hayes, "U-Mo Fuels Handbook Version 1.0," Argonne National Laboratory, Argonne, Illinois, June 2006.

[12] Private communication with Gerard Hofman of Argonne National, RERTR.

[13] Inspection Certificate 3.1B, Certificate No. 200780, Böhler Bleche, GMBH, dated February 2, 2001.

[14] E.W. Lemmon, M.O. McLinden and D.G. Friend, "Thermophysical Properties of Fluid Systems" in NIST Chemistry WebBook, NIST Standard Reference Database Number 69, Eds. P.J. Linstrom and W.G. Mallard, National Institute of Standards and Technology, Gaithersburg MD, 20899, http://webbook.nist.gov.

[15] G.C. Allen, Jr., L. Clark, Jr., J.W. Gosnell, D.D. Lanning, "The Reactor Engineering of the MITR-II Construction and Startup," MITNE-186, Nuclear Engineering Dept., Massachusetts Institute of Technology, Cambridge, Massachusetts, June 1976.

[16] MITR-II "Core Housing - Absorber Spider," drawing R3S-27-4 rev. J, MIT Nuclear Reactor Laboratory, Massachusetts Institute of Technology, Cambridge, Massachusetts, revision dated August 19, 1975

[17] MITR-II "Core Housing - Absorber Spider," drawing R3S-12B-4 rev. B, MIT Nuclear Reactor Laboratory, Massachusetts Institute of Technology, Cambridge, Massachusetts, revision dated February 21, 1977 to drawing dated May 13, 1976.

[18] MITR-II "Control Blade Assembly – Control Blade," drawing R3C-28-4 rev. C, MIT Nuclear Reactor Laboratory, Massachusetts Institute of Technology, Cambridge, Massachusetts, revision dated May 12 1975 to drawing dated August 6, 1973.

[19] MITR-II "Control Blade Mechanism," drawing R3C-41-4 rev. D, MIT Nuclear Reactor Laboratory, Massachusetts Institute of Technology, Cambridge, Massachusetts, revision dated August 1980 to drawing dated 1976.

[20] MITR-II "Control Blade - Inner Section," drawing R3C-42-4 rev. A, MIT Nuclear Reactor Laboratory, Massachusetts Institute of Technology, Cambridge, Massachusetts, March 8, 1976.

[21] MITR-II "Control Blade – Outer Section," drawing R3C-43-4 rev. B, MIT Nuclear Reactor Laboratory, Massachusetts Institute of Technology, Cambridge, Massachusetts, March 8, 1976.

[22] MITR-II "Core Housing – Cadmium Inserts," drawing R3S-28-3 rev. D, MIT Nuclear Reactor Laboratory, Massachusetts Institute of Technology, Cambridge, Massachusetts, revision dated August 19, 1975 to drawing dated January 13, 1972.

[23] MITR-II "Core Housing – Insert-Absorber Spider," drawing R3S-120-2 rev. A, MIT Nuclear Reactor Laboratory, Massachusetts Institute of Technology, Cambridge, Massachusetts, May 28, 1976.

[24] MITR-II "1% Boron- S.S. Absorber Spider - Inserts," drawing R3S-138-1 rev. A, MIT Nuclear Reactor Laboratory, Massachusetts Institute of Technology, Cambridge, Massachusetts, July 15, 1977.

[25] MITR-II "Core Housing - Spider," drawing R3S-16-2 rev. E, MIT Nuclear Reactor Laboratory, Massachusetts Institute of Technology, Cambridge, Massachusetts, revision dated October 24, 1974 to drawing dated May 19, 1970.

[26] MITR-II "Solid Dummy Element – Type 'B'," drawing R3F-15-4 rev. B, MIT Nuclear Reactor Laboratory, Massachusetts Institute of Technology, Cambridge, Massachusetts, February 24, 1976.

[27] MITR-II "Reg Rod Assembly," drawing R3C-25-4 rev. C, MIT Nuclear Reactor Laboratory, Massachusetts Institute of Technology, Cambridge, Massachusetts.

[28] MITR-II "Core Housing – Housing Body," drawing R3S-14-5 rev G, MIT Nuclear Reactor Laboratory, Massachusetts Institute of Technology, Cambridge, Massachusetts, revision dated May 12, 1975 to drawing dated December 22, 1969.

[29] MITR-II "Core Housing – Lower Grid Plate," drawing R3S-15-4B rev. B, MIT Nuclear Reactor Laboratory, Massachusetts Institute of Technology, Cambridge, Massachusetts, revision dated September 12, 1974 to drawing dated October 21, 1971.

[30] MITR-II "Core Tank – Core Housing Assembly," drawing R3S-3-5 rev I, MIT Nuclear Reactor Laboratory, Massachusetts Institute of Technology, Cambridge, Massachusetts, revision dated May 12, 1975 to drawing dated 1970.

[31] T.H. Newton, N. Horelick, P. Romano, B. Forget, E.E. Pilat, E.H. Wilson, B. Dionne, A. Bergeron, and J. Stevens, "LEU Conversion activities at the MIT Research Reactor: Use of Neutronic Models for Safety Analysis," Proceedings of the RERTR Conference, Lisbon, Portugal, Oct. 2010.

[32] J.G. Stevens, "The REBUS-MCNP Linkage," ANL/RERTR/TM-08-04, Argonne National Laboratory, April 2008.

[33] N. Hanan, B. Dionne, "Impact of Photoneutrons on Transients for the MITR and MURR HEU and LEU Cores," Proceedings of the RERTR Conference, Lisbon, Portugal, Oct. 2010.

[34] M.M. Bretscher, "Perturbation-Independent Methods for Calculating Research Reactor Kinetic Parameters," ANL/RERTR/TM-30, December 1997.

[35] Control blade 1 calibration data, unpublished MITR-II logbook data dated 3/16/76, MITR-II, Massachusetts Institute of Technology, Cambridge, Massachusetts.

[36] Control blade 3 calibration data, unpublished MITR-II logbook data dated 3/15/76, MITR-II, Massachusetts Institute of Technology, Cambridge, Massachusetts.

[37] Control blade 5 calibration data, unpublished MITR-II logbook data dated 3/16/76, MITR-II, Massachusetts Institute of Technology, Cambridge, Massachusetts.

[38] Control blade 2 calibration data, unpublished MITR-II logbook data dated 11/21/76, MITR-II, Massachusetts Institute of Technology, Cambridge, Massachusetts.

[39] Control blade 4 calibration data, unpublished MITR-II logbook data dated 11/17/76, MITR-II, Massachusetts Institute of Technology, Cambridge, Massachusetts.

[40] Control blade calibration procedure, unpublished MITR-II logbook entry dated 3/20/76, MITR-II, Massachusetts Institute of Technology, Cambridge, Massachusetts.

[41] A.G. Croff, "A User's Manual for the ORIGEN2 Computer Code," ORNL/TM-7175, Oak Ridge National Laboratory (1980).

[42] A.P. Olson, "A User's Guide for the REBUS-PC Code, Version 1.4," ANL/RERTR/TM-32, Argonne National Laboratory, December 2001.

[43] A. Olson and T. Newton, "Highly Detailed Triangular Mesh Diffusion Theory vs. Monte Carlo: Modeling the MIT Research Reactor," Proceedings of the Research Reactor Fuel Management (RRFM) Conference, Hamburg, Germany, March 2008.

[44] T.H. Newton, Jr., A.P. Olson, and J.A. Stillman, "Reactor Core Design and Modeling of the MIT Research Reactor for Conversion to LEU," Proceedings of the RERTR Conference, Prague, Czech Republic, September, 2007.

[45] J.A. Bernard, Jr., S.M. Thesis, "MITR-II Fuel Management, Core Depletion, and Analysis: Codes Developed for the Diffusion Theory Program CITATION," Massachusetts Institute of Technology, Cambridge, Massachusetts, 1979.

[46] "MCNP - A General Monte Carlo N-Particle Transport Code, Version 5 User's Guide Manual," X-5 Monte Carlo Team, LA-UR-03-1987, Los Alamos National Laboratory, April 2003.

[47] Z. Xu, P. Hejzlar, and M.S. Kazimi, "MCODE, Version 2.2 — An MCNP-ORIGEN Depletion Program," Center for Advanced Nuclear Systems," Massachusetts Institute of Technology, Cambridge, Massachusetts, April 2006.

Nuclear Engineering Division
Argonne National Laboratory
9700 South Cass Avenue, Bldg. 208
Argonne, IL 60439-4842

www.anl.gov